GEORGIA INSTITUTE OF TECHNOLOGY
OFFICE OF CONTRACT ADMINISTRATION
SPONSORED PROJECT INITIATION

Date: 2/16/77

Project Title: "Low Energy Experiment to Measure a Weak Coupling of the Neutrino Current."

Project No: B-484

Project Director: Mr. T. P. Lang

Sponsor: National Science Foundation

Agreement Period: From 1/1/77 Until 6/30/78

Type Agreement: Grant No. PHY77-03680

Amount: $179,600 (B-484 - $137,913
G-41-654 - $41,687)

Reports Required: Annual Technical Letter, Final Technical Report

Sponsor Contact Person (s):

Technical Matters

Contractual Matters
(thru OCA)

James L. Bostick
Grants Officer
National Science Foundation
Washington, D. C. 20550

Defense Priority Rating: n/a

Assigned to: Applied Sciences Laboratory (School/Laboratory)

COPIES TO:

Project Director
Division Chief (EES)
School/Laboratory Director
Dean/Director—EES
Accounting Office
Procurement Office
Security Coordinator (OCA)
Reports Coordinator (OCA)

Library, Technical Reports Section
Office of Computing Services
Director, Physical Plant
EES Information Office
Project File (OCA)
Project Code (GTRI)
Other

Posted 10/31/78 OHL

GEORGIA INSTITUTE OF TECHNOLOGY
OFFICE OF CONTRACT ADMINISTRATION

SPONSORED PROJECT TERMINATION

Date: 10/31/78

Project Title: Low Energy Experiment to Measure a Weak Coupling of the Neutrino Current

Project No: B-484(Sub-project is G-41-654/Ahrens/Physics)

Project Director: Dr. T. P. Lang, Jr.

Sponsor: National Science Foundation

Effective Termination Date: 6/30/78

Clearance of Accounting Charges: All cleared

Grant/Contract Closeout Actions Remaining:

- _ Final Invoice and Closing Documents
- X Final Fiscal ~~Report~~ Accounting (FCTR)
- _ Final Report of Inventions
- _ Govt. Property Inventory & Related Certificate
- _ Classified Material Certificate
- _ Other _____

CONTINUED BY: B-509 (Sub-project is G-41-668/Ahrens/Physics)

Assigned to: ASL/APB (School/Laboratory)

COPIES TO:

- Project Director
- Division Chief (EES)
- School/Laboratory Director
- Dean/Director—EES
- Accounting Office
- Procurement Office
- Security Coordinator (OCA) ✓
- Reports Coordinator (OCA)
- Library, Technical Reports Section
- Office of Computing Services
- Director, Physical Plant
- EES Information Office
- Project File (OCA)
- Project Code (GTRI)
- Other G-41-654/distribution

CA—4 (3/76)

FR

EES/GIT PROJECT B–484

LOW ENERGY EXPERIMENT TO MEASURE A WEAK COUPLING OF THE NEUTRINO CURRENT

NSF GRANT PHY77–03680

JUNE 1978

GEORGIA INSTITUTE OF TECHNOLOGY

Engineering Experiment Station

Atlanta, Georgia 30332

1978

Progress Report NR4-B
(EES/GIT Project B-484)

"LOW ENERGY EXPERIMENT TO MEASURE A WEAK COUPLING OF THE NEUTRINO CURRENT"

Final Technical Report, NSF Grant PHY77-03680

June 1978

Authors:

R. M. Ahrens
F. T. Avignone, III (Univ. S. Carolina)
S. M. Blankenship
D. S. Harmer
T. P. Lang
A. M. Rushton (Univ. Massachusetts)
M. H. Wood

T. P. Lang
Project Director and
Principal Investigator
for Experimental Aspects

R. M. Ahrens
Principal Investigator
for Theoretical Aspects

GEORGIA INSTITUTE OF TECHNOLOGY

Atlanta, Georgia

Abstract

The achievements of the Georgia Tech neutrino research group for the period January 1977 through December 1977 are described in this progress report. The goal of the present research activities is to perform an experiment in which features of the neutral weak current are investigated via the reaction of reactor antineutrinos with deuterons. The experiment requires several identical modules, each consisting of a central deuterated scintillator surrounded by a second lithium-6 loaded scintillator. All modules must be within a massive multilayered bulk shield which in turn is surrounded by an active scintillator anticoincidence cosmic ray shield.

Third generation bulk and cosmic ray shields have been built and evaluated. Two full size prototype dual concentric modules have been constructed and evaluated. Experimentation has been concentrated upon the measurement of those factors affecting the counting time for the proposed experiment. Particular emphasis was directed at achieving an accurately calibrated low energy detection capability with absolute minimum background. The effects of cosmic rays, natural radioactivity and photomultiplier tube noise have been investigated extensively. The results are very encouraging and show that an upper limit for the counting time required for a measurement of the $\bar{\nu}(d, n+p)\nu$ reaction cross section to a precision of 25% can be as short as 62 days. The extended counting time required to achieve a more precise measurement is well within reasonable limits.

TABLE OF CONTENTS

LIST OF FIGURES

List of Figures (Continued)

LIST OF TABLES

Chapter I

INTRODUCTION

This report has been prepared for the National Science Foundation to document progress toward the goals of the neutrino research project at Georgia Tech. The ultimate goal of the present research program is to perform an experiment in which features of the neutral weak current are investigated via the reaction of reactor antineutrinos with deuterons.

The goal is not only to detect the existence of the weak neutral current by observation of the low energy electron antineutrino disintegration of the deuteron, but also to obtain an accurate measurement of the cross section. The experiment is designed to define an antineutrino induced deuteron disintegration event signature which is sufficiently restricted to avoid most extraneous events, and to allow accurate measurement of the experimental parameters such as efficiencies, energy thresholds, etc.

In the antineutrino disintegration of the deuteron,

$$\bar{\nu}_e + D \rightarrow p + n + \bar{\nu}'_e \ , \qquad (1)$$

the detectable products are a proton and a neutron. The experimental arrangement allows the direct detection of the proton and the measurement of the energy of the proton deposited in the deuterated target scintillator. The neutron is detected after a migration and thermalization time in the concentric lithium loaded scintillator. The energy recorded from the neutron detector is not that of the neutron, but the energy of the alpha/triton pair produced in the exothermic reaction of the neutron and a ^{6}Li nucleus,

$$n + {}^{6}Li \rightarrow {}^{4}He + {}^{3}H + 4.8 \text{ MeV} . \qquad (2)$$

Figure 1 is a schematic of the detection scheme.

This second year of our current effort has been devoted to establishing and examining the criteria bearing on the probable outcome or "feasibility" of the proposed experiment, a direct continuation of the program discussed in the previous progress report NR4-A ("Low Energy Experiment to Measure a Weak Coupling of the Neutrino Current," January 1977, Final Technical Report of NSF Grant PHY75-21295). Particular emphasis was directed at achieving a low energy detection capability with absolute minimum background.

As originally proposed the experiment would be performed with six identical modules, each consisting of a central deuterated scintillator surrounded by a second lithium-6 loaded scintillator. All modules must be inside a massive multilayered bulk shield which in turn is surrounded by an active scintillator anticoincidence cosmic ray shield. Third generation bulk and cosmic ray shields have been built and evaluated. Two full size prototype dual concentric modules have been constructed and evaluated.

Feasibility studies have been concentrated upon the measurement of those factors affecting the counting time for the proposed experiment. The effects of cosmic rays, natural radioactivity and electronic noise have been investigated by calculational techniques and experimentally with NaI detectors, neutron detectors and the prototypes. The serendipitous discovery that acrylic plastics do not degrade the lithium-loaded scintillator has considerably reduced the complexity of module fabrication and will improve the light collection properties of the outer detector.

$$\bar{\nu}_e + D \longrightarrow P + N + \bar{\nu}_e$$

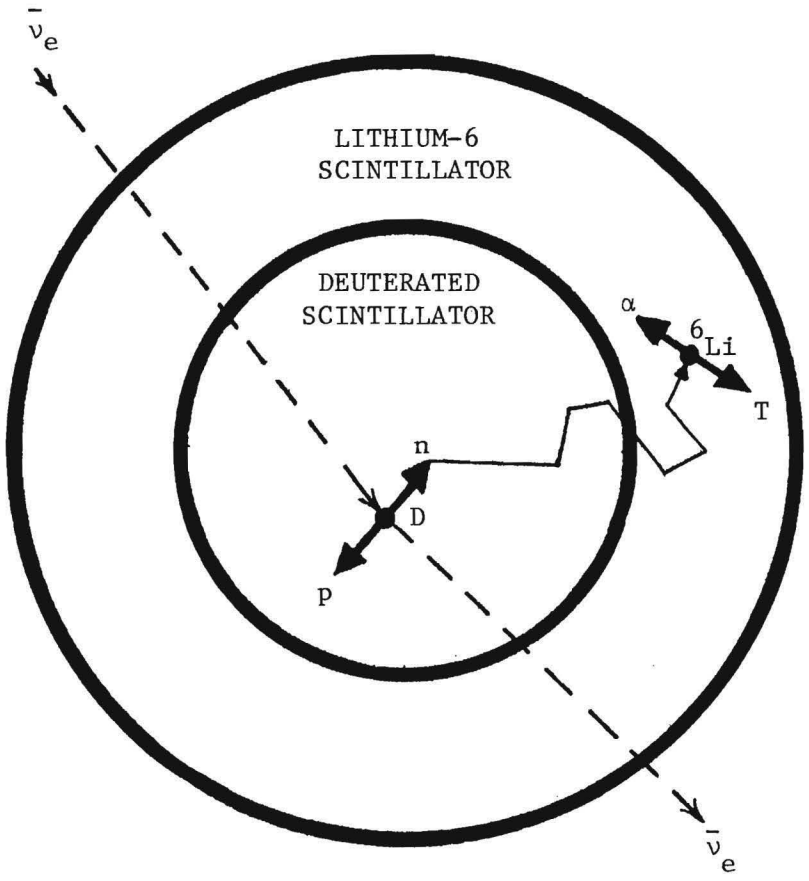

FIGURE 1. DETECTION SCHEME

The following two chapters are devoted to detailing the accomplishments of the researchers during the present reporting period. An analysis of the feasibility criteria is presented in the final chapter. This analysis, derived from two years of research, shows that an upper limit for the counting time required for a measurement of the $\bar{\nu}(d, n+p)\bar{\nu}$ reaction cross section to a precision of 25% can be as short as 62 days. The extended counting time required to achieve a more precise measurement is well within reasonable limits.

Chapter 2

CALCULATIONAL ACTIVITIES

The following three research efforts involving computer calculations were pursued in the course of the report period.

Neutrino Spectrum and Cross Section Calculation

In the years since the most recent calculation of the antineutrino spectrum from fission product decays, a considerable body of further spectrographic detail, nuclear mass measurements and fission product systematics had accumulated. Since the spectral shape is sensitive to these details, another calculation incorporating this new knowledge was completed. Questions concerning the antineutrino-deuteron weak neutral current interaction cross section had also arisen, primarily from the publication of several apparently different cross sections for the reaction. An effort was mounted to resolve the differences in cross section by recalculating the cross section using the new spectrum with the method of each author. Subtle theoretical errors were discovered in some of the results published by other groups.

The paper in Appendix I displays the results of the new spectrum calculation and the resolution of the differences between the calculated cross sections. The value for the cross section was calculated to be 7.4×10^{-45} cm^2 using the new spectrum.

Gamma-Ray Response of Liquid Scintillators

The energy calibration of the electron response of liquid scintillators is most easily obtained from the collection of pulse height spectra while the detector is irradiated with monoenergetic gamma rays. The association of the resultant pulse height spectra with particular energies is

accomplished by comparison with calculations of the spectra. These calculated spectra are obtained using a Monte Carlo computer program which was further developed during the course of the report period.

Some unphysical results in the low energy end of some calculated spectra were traced to an inappropriate random number generator. The problem was corrected, and the earlier unphysical results disappeared after this change.

The computer program was changed to include the effects of the non-linearity with energy of the light output per energy deposited in the scintillator. This resulted in the calculation of the spectrum of the relative numberof photons emitted from the scintillator as a function of the interaction energy rather than the spectrum of energy deposited in the scintillator.

To increase the efficiency of the program, alternative methods of selecting the Compton scattering angle were investigated. The Neyman rejection method was found to be most suitable, and significantly reduced the amount of time required for the calculations.

To include the effects of system resolution, a guassian resolution function was introduced. The width of the resolution function was allowed to vary either directly with energy or directly with the square root of the energy. Investigation is continuing to determine which of these is more appropriate for calculations of spectra in the range of energies of interest to this project.

Response Function of NaI Detector

The response function of a NaI detector permits one to infer the omnidirectional gamma flux from the pulse height spectrum obtained in

the detector. An approximate method was used to obtain the gamma ray flux within the experimental shield as reported in the previous progress report NR4-A. The effort to produce a precise response function by Monte Carlo methods has continued.

During this reporting period, the identification of the inappropriate random number generator and its repair was accomplished. The Neyman rejection method was incorporated into the program. A conclusion of this effort is expected shortly.

Chapter 3

EXPERIMENTAL INVESTIGATIONS

An important objective of the program was the experimental evaluation and optimization of the various options for the configuration and design of the detector system. The deuterated scintillator, lithium-6 loaded scintillator, bulk shield and cosmic ray umbrella are discussed in this chapter.

The Deuterated Scintillator

One of the main keys to the success of the proposed experiment is the highly deuterated liquid scintillator which serves as the target scintillator volume. It is the inner region of the concentric two-region detector. A high degree of deuteration of the target scintillator is very important for several reasons. First, the maximum number of deuterium target atoms should be contained in the minimum volume so that the overall shielded volume is kept to a minimum. Second, the gamma ray background rate in a scintillator is directly proportional to the volume. An increase in the fraction of deuteration by a factor of two, for example, doubles the signal to noise ratio. Third, one source of background, which is reactor associated, will be caused by the inverse beta decay of protons. This background is, of course, directly proportional to the number of ordinary hydrogen atoms in the target scintillator and is minimized by maximum deuteration.

The deuterated scintillator, with a solvent of 95% deuterated octane, has a light output of 80% of that of the scintillator known as NE 213, which is a high-light-output organic scintillator produced by Nuclear Enterprises, Inc. and which is frequently used as a reference scintillator.

The deuterated scintillator was synthesized by multiple exchange with deuterium oxide over a nickel-kieselguhr catalyst at high temperature and then purified by fractional distillation. Perdeutero-naphthalene was also synthesized, since its use as a secondary solvent to improve scintillation response was found to be substantial. The fraction of deuteration was determined by mass spectrometry while the purity was determined by infrared and ultraviolet spectroscopy. The fraction of deuteration was also measured by observing the proton concentration by nuclear magnetic resonance (NMR). These spectroscopic studies were capable of determining the hydrogen fraction with an accuracy of one part in one hundred. This means, for example, that one can distinguish between 4.0% and 4.8% hydrogen which corresponds to 96.0% and 95.9% deuterium respectively.

The optimization of the concentrations of primary solute, wavelength shifter and secondary solute in a N-octane based liquid scintillator were performed. These concentrations were varied in a full size central acrylic cell, including the light pipes, and the relative pulse heights of the energy distributions of Compton electrons due to standard gamma rays were measured. An XP 2041 Amperex photomultiplier tube was coupled to each end of the target scintillator cell assembly in the normal manner. A fast linear gate was used to suppress the photomultiplier tube noise and the Compton distributions from the standard gamma rays in ^{60}Co, ^{54}Mn and ^{137}Cs were observed as a function of the concentrations of PPO, BIS-MSB and naphthalene. With each new concentration, the solution was bubbled 30 minutes with helium to remove dissolved oxygen and 5 minutes with argon to establish a clean atmosphere in the void in the cell. The following concentrations by weight were found to maximize the light output:

0.45% PPO, 0.01% BIS-MSB and 3.5% naphthalene. The total composition of the deuterated target-scintillator is given in Table 1.

The response of the deuterated scintillator assembly was measured by observing the Compton energy distributions of the 116, 274, and 662 keV gamma rays in the decays of ^{139}Ce, ^{203}Hg and ^{137}Cs respectively. The general features and the quality of these spectra are very similar to those discussed in the previous progress report.

The energy calibration of the deuterated target scintillator is critically important in this experiment. Several methods have been attempted; however, no method was found which was nearly as simple or practical as the use of the Compton distribution due to gamma rays. Gamma ray sources can be inserted into the shielded region and can be sealed so as not to contaminate the shield or target. The major difficulty with this method is that the so-called Compton peak in the distribution is broad and has a shape which is energy dependent. In addition, the leading edge of the distribution also has an energy dependent shape. While the spectra are very simple to acquire, their interpretation is far from straightforward and in fact is extremely energy dependent.

The accurate interpretation of such spectra is made possible by a detailed Monte Carlo calculation which contains experimental Compton scattering cross sections for each energy, selects a Compton scattering angle using a routine which is designed to reproduce the Klein-Nishina distribution and which allows for multiple Compton scattering events. This code was written for the specific geometry of the present target and gives results very similar to those actually observed using calibration gamma rays. The light collection efficiency and other effects which tend to smear the energy spectra are accounted for in the Monte Carlo calculations

TABLE 1

COMPOSITION OF DEUTERATED SCINTILLATOR

Chemical Name	Formula	Molecular Weight	% By Weight
Deuterated n-octane	$CD_3(CD_2)_6CD_3$	132	92.2 ± 0.08
Deuterated naphthalene	$C_{10}D_8$	136	3.4 ± 0.002
bis-MSB	$C_{24}H_{22}$	310	0.01 ± 0.00001
PPO	$C_{15}H_{11}NO$	221	0.45 ± 0.0003
n-octane	$CH_3(CH_2)_6CH_3$	114	3.8 ± 0.003
Naphthalene	$C_{10}H_8$	128	0.1 ± 0.0001

Atomic Composition

H	$31.92 \pm 0.02 \times 10^{20}$ atoms/cm^3
D	$648.0 \pm 0.5 \times 10^{20}$ atoms/cm^3
C	$311.7 \pm 0.2 \times 10^{20}$ atoms/cm^3
N	$0.103 \pm 0.00001 \times 10^{20}$ atoms/cm^3
O	$0.103 \pm 0.00001 \times 10^{20}$ atoms/cm^3

Density = 0.842 g/cm^3

by use of an empirically determined smearing routine. The noise suppression achieved by use of the fast linear gate allows the proton window to be set at about 100 keV of proton recoil energy, while the comparison of the calibration gamma ray spectra with those of the Monte Carlo calculations allows the accurate determination of the energy corresponding to this threshold.

The determination of the correspondence between proton recoil energies and those due to Compton electrons is required. A measurement of this relative response was accomplished using low energy protons from a van de Graaff accelerator introduced through a 0.1 mil nickel window and Compton electrons from gamma ray sources. The ratio of electron response to proton response was determined to be 8 ± 2, where the major source of error consists of the uncertainty in proton energy introduced by the beam interaction with the window. Neutron scattering can better determine this ratio by reducing the effect of the window. An experiment to determine this using n-p elastic scattering has been designed to be run at ORELA (Oak Ridge Electron Linear Accelerator) using the standard time of flight techniques to separate recoil spectra due to neutrons of a given energy. Plans have been discussed with Dr. S. Raman at ORELA and the experiment has been scheduled.

The combination of the techniques and results discussed above will allow the accurate determination of the proton energy threshold of the detector and its energy calibration. In addition, they afford a simple method of monitoring the gains of the target photomultiplier tubes using standard gamma ray spectroscopy techniques. We conclude that all of the difficulties associated with the deuterated central detector have been overcome, with the only outstanding measurements being those planned at ORELA. These are critical for the accurate interpretation of the

final data; however, the measurements can be made or remade at any time without holding up progress on the cross section measurement.

The Lithium-6 Loaded Scintillator

The second scintillator developed specifically for the proposed experiment is a lithium-6 loaded organic liquid scintillator. Two, low molecular weight lithium containing compounds have been synthesized in extremely pure form which can be added in quantities of up to 10.5 moles/kg of scintillator solvents. The lithium compounds are specifically lithium secondary butoxide and lithium tertiary butoxide. The neutron is then detected by the reaction $^{6}Li(n,\alpha)^{3}H$ with the α-particle and triton being observed in the scintillator with a total kinetic energy of 4.78 MeV. The cross section for thermal neutrons is 942 barns which results in this scintillator being extremely efficient as a neutron detector. As discussed in NR4-A, Monte Carlo calculations show that the outer scintillator of the dimensions being considered will have an efficiency of about 0.95 for detecting the neutrons produced in the reaction, $\bar{\nu}_e + D \rightarrow p + n + \bar{\nu}_e$ where $\bar{\nu}_e$ energy spectrum is that from a nuclear reactor. The result of the Monte Carlo calculations for the spacial and temporal distributions of the capture of the neutrons for the proposed geometry is shown in Figures 2A and 2B of the previous progress report (NR4-A).

The lithium butoxide is synthesized by boiling Butyl alcohol and condensing it and allowing it to flow over a small piece of lithium metal. This compound is extremely reactive and must be synthesized and kept in an inert atmosphere. The reaction with the alcohol produces hydrogen which combines with metallic lithium which produces small quantities of lithium hydride. Helium gas is bubbled through the boiling solution

which stimulates the decomposition of the hydride by the alcohol and carries off the hydrogen. The resulting compound consists of a slush solution of lithium butoxide in alcohol along with small quantities of lithium hydride and lithium hydroxide.

Very minute traces of oxygen will form a yellow compound with a strong absorption in the blue and ultra-violet region of the spectrum. Small traces of moisture will cause the precipitation of a white substance which is probably lithium hydroxide. In both cases the scintillator is degraded. Hence, extreme care in synthesizing, transferring and packaging is of the utmost importance. In our work described in Chapter 3, an ordinary proton rich scintillator was used in the outer region of the two region detector. The geometry resulted in sufficient light collection for good energy resolution, so that the full energy peak of the α-particle and triton from the reaction $^{6}Li(n,\alpha)^{3}H$ would be covered by a reasonably narrow window. This significantly reduces the background due to random counts in the outer region. In this preliminary work, the container was fabricated from acrylic which results in simplicity and allows the use of total internal reflection in the light collection scheme. The composition of the lithium-6 loaded scintillator is given in Table 2. The response of the scintillator to the spectrum of neutrons from a Pu-Be source is shown in Figure 2 while the response to thermal neutrons is given in Figure 9 of the previous progress report.

Experimental Studies of Prototype Modules

The detection of reaction (1) without the concurrent detection of extraneous background events requires a signature definition which mitigates against the background. Three experimental parameters are used to

TABLE 2

COMPOSITION OF LITHIUM-6 LOADED SCINTILLATOR

(1 mole ^{6}Li-t-Butoxide per liter)

Chemical Name	Formula	Molecular Weight	% By Weight
n-Octane	$CH_3(CH_3)_6CH_3$	114	86.7
PPO	$C_{15}H_{11}NO$	221	0.41
bis-MSB	$C_{24}H_{22}$	310	0.01
Naphthalene	$C_{10}H_8$	128	3.16
^{6}Li-Butoxide	$^{6}LiOC_4H_9$	79	9.36
^{7}Li-Butoxide	$^{7}LiOC_4H_9$	80	0.39

Atomic Composition

H	733.0×10^{20}	atoms/cm^3
^{6}Li	5.8×10^{20}	atoms/cm^3
^{7}Li	0.24×10^{20}	atoms/cm^3
C	334.5×10^{20}	atoms/cm^3
N	0.09×10^{20}	atoms/cm^3
O	6.1×10^{20}	atoms/cm^3

Density = 0.8105 gm/cm^3

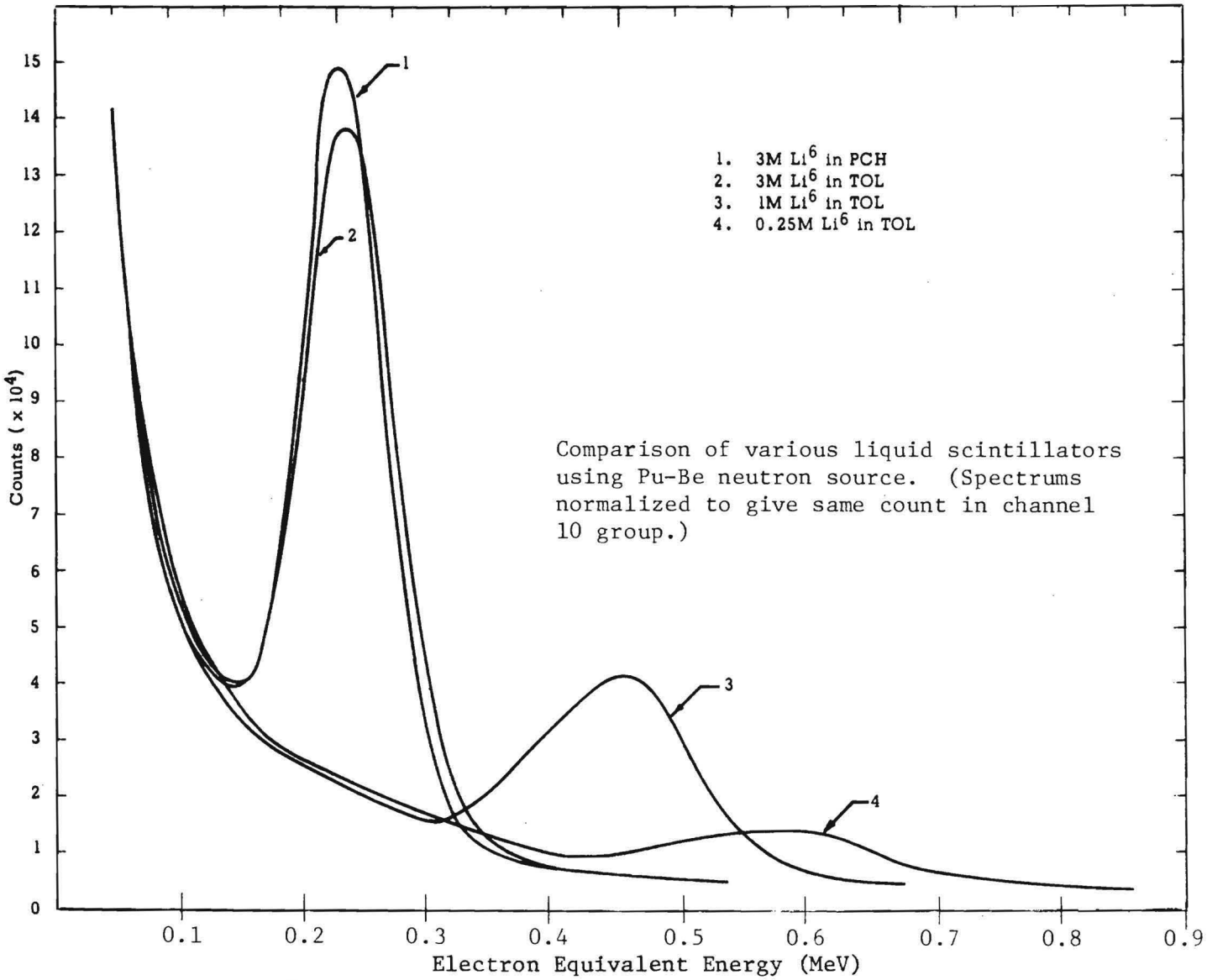

FIGURE 2. ^{6}Li LIQUID SCINTILLATOR RESPONSE TO Pu-Be NEUTRONS

delimit the signature of the antineutrino-deuteron reaction. They are:

1. Proton Energy Window = ΔE_p = 0.1 to 1.0 MeV;

2. Neutron Energy Window = ΔE_n = 0.30 to 0.65 MeV (electron equivalent energy);

3. Capture Time Window = $\Delta\tau$ = 0.1 to 33 microseconds.

In addition, the rate of extraneous signatures is reduced by the rejection of events which are promptly coincident in both detectors and the rejection of signatures following the detection of an event in the cosmic ray anticoincidence detectors.

The background signature event rate B can be expressed as the sum

$$B = B_1 + B_2 + B_3 , \qquad (3)$$

where B_1 includes all observed correlated events producing the event signature (i.e., from reactions 1a through 1g, Section B, page 8, NR4-A), B_2 all observed correlated events which synthesize the signature, such as the scattering of a gamma ray from one detector to another, and B_3 all observed signatures due to the chance synthesis by uncorrelated events.

The rate B_1 consists of the sum of rates due to the neutron, gamma ray and antineutrino fluxes within the shield. The largest term of this sum is the rate of photodisintegration of the deuteron, for the ratio of neutron to gamma ray fluxes is low.

The rate B_2 also consists of a sum of rates, each due to the scattering of different particles. The neutron portion is negligible compared to the others, and for the same reason of reduced flux. The rejection of correlated scattering events is accomplished by the rejection of signatures

which are in prompt coincidence in the two detectors of a module. This eliminates those scattering events caused by swift particles.

The chance rate B_3 consists of a product of the rate of events in each of the two detectors in a module. All sources of events contribute, including electronic noise.

These rates are defined for the entire multimodule experiment. The corresponding rates within a single module are distinguished below as lower case b's.

First Prototype of Experimental Module

To examine the characteristics of a complete, two detector module a prototype was constructed of acrylic. The details and its dimensions and construction are shown in Figure 3. Two Amperex XP2041 photomultiplier tubes were mounted on the inner detector light pipes. Two nine inch diameter Amperex 57AVP photomultiplier tubes were mounted on the light pipes at the ends of the module. The outer light pipes consist of cylindrical volumes filled with pure nonscintillating solvent, capped by solid pieces of acrylic which direct the light to the photocathodes of the photomultiplier tubes. Access to the inner photomultiplier tubes was available through slots milled in the solid light pipes on each end. Details of the light pipes for the outer detector are shown in Figure 4.

The entire module was inserted in Shield II (see Figure 5), the second in a series of increasingly enlarged shields. The detector modules of the experiment must be adequately shielded from reactor radiation, cosmic radiation and the natural radioactive contamination backgrounds. Reactor associated radiations other than antineutrinos can contribute falsely to the observed signature event rates, while the cosmic ray and

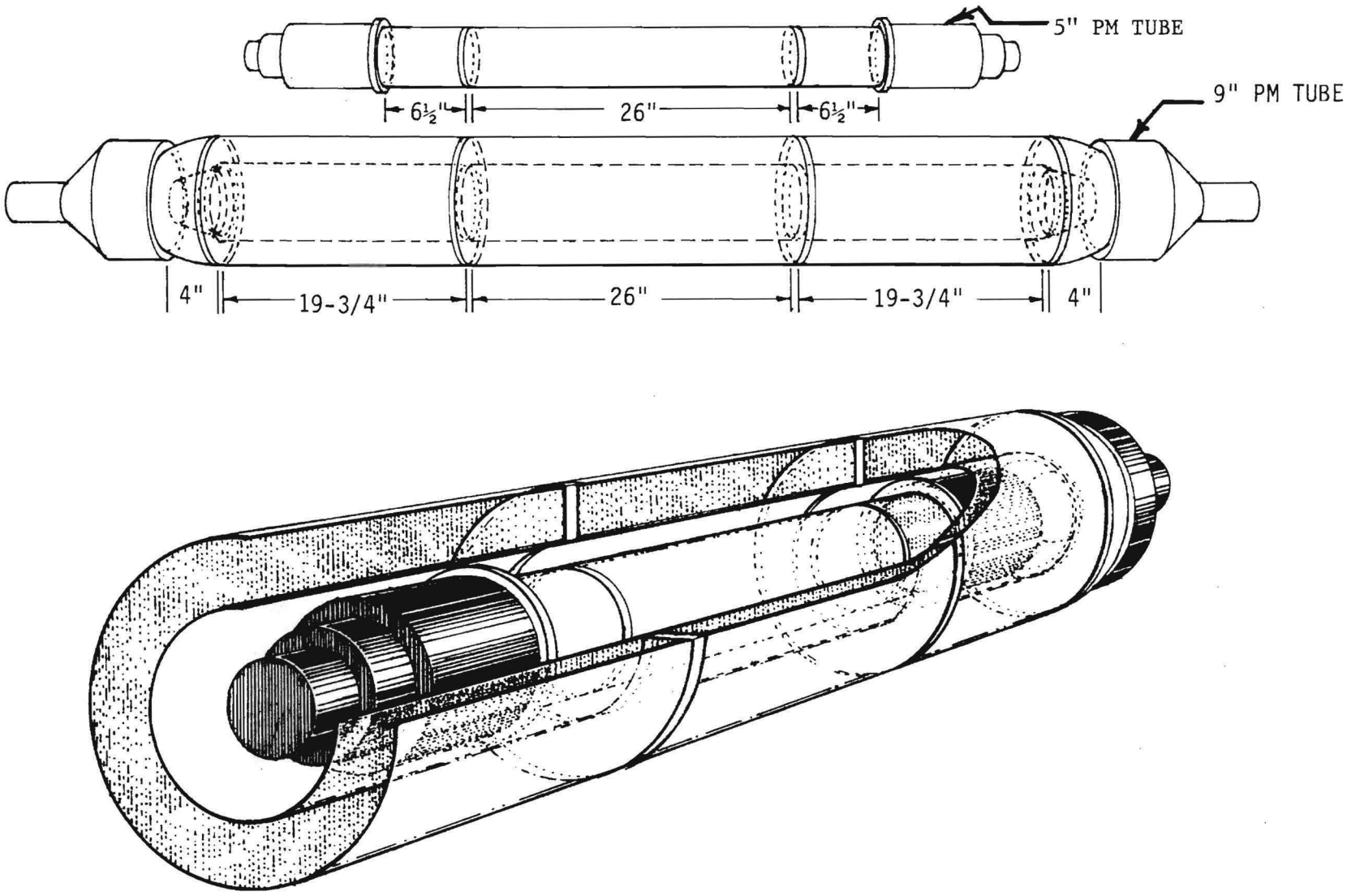

FIGURE 3. DETAILS OF THE PROTOTYPE DETECTORS AND MODULE

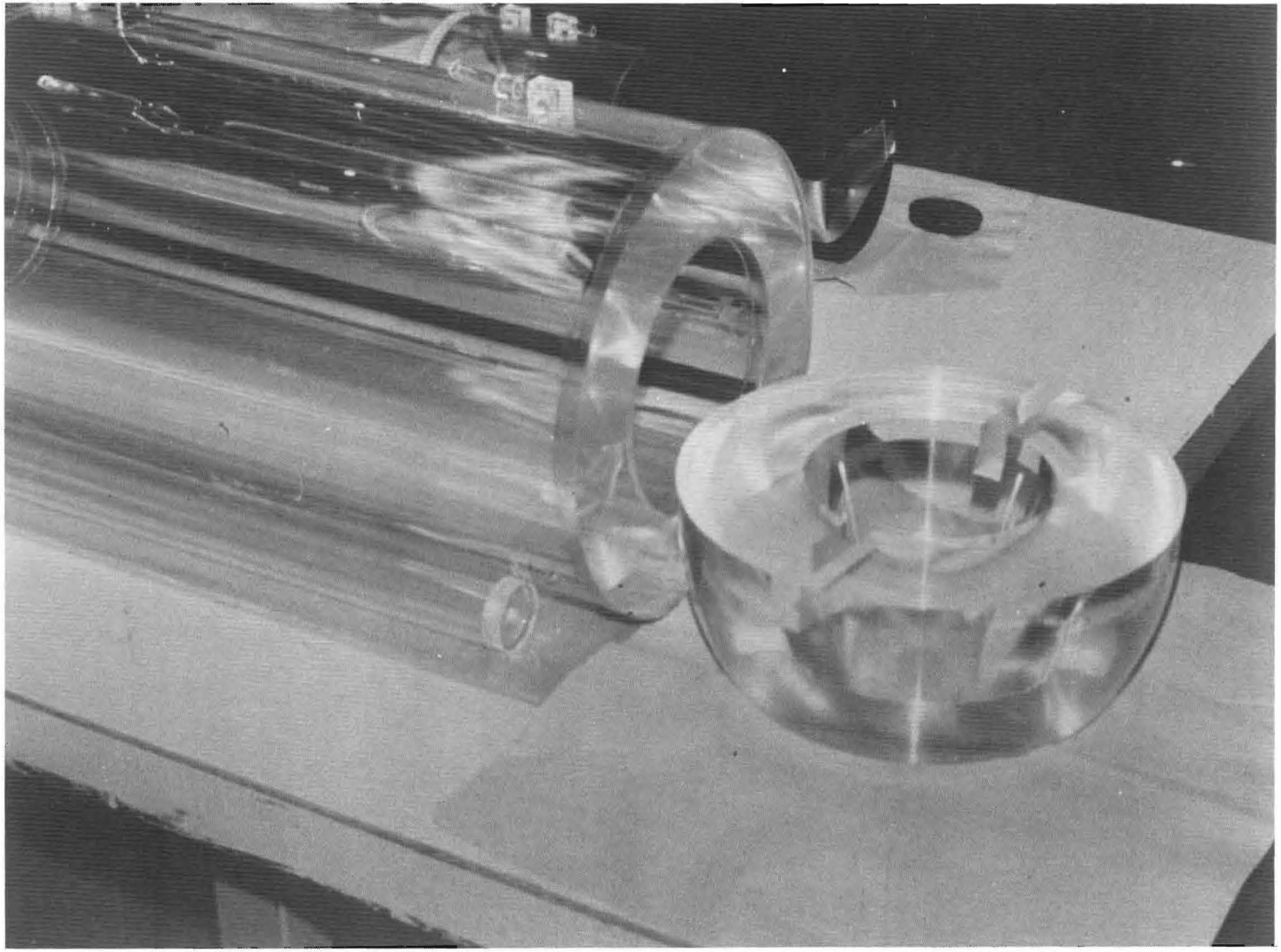

FIGURE 4. PHOTOGRAPH OF DISASSEMBLED OUTER DETECTOR LIGHT PIPE

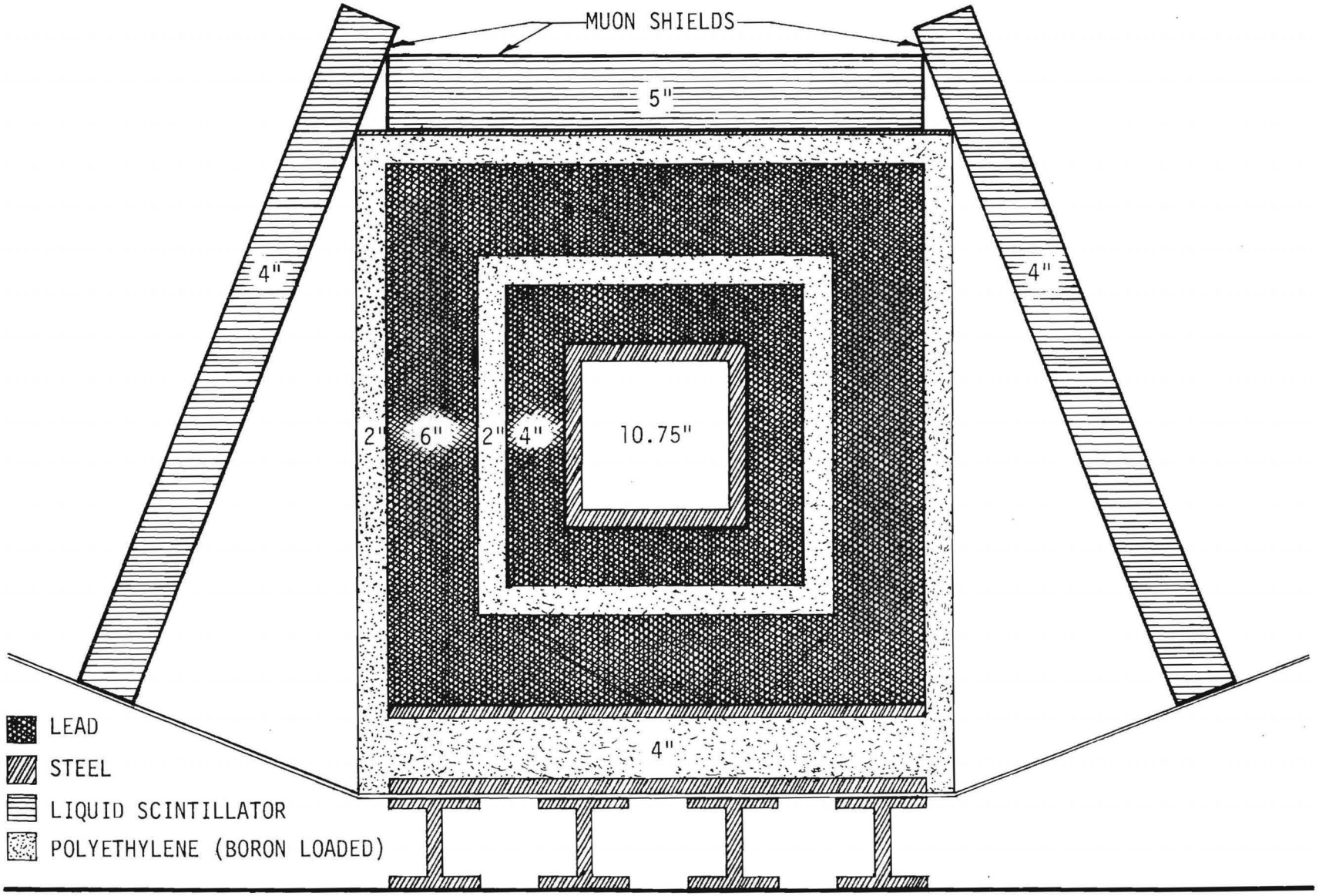

FIGURE 5. SCHEMATIC CROSS SECTION OF SHIELD II

natural radiation backgrounds can contribute to the continuous background which strongly governs the length of time required for the experiments.

The electronic system which processed the photomultiplier signals from the module and the cosmic ray umbrella (CRUMB) is shown schematically in Figure 6. This system allowed investigation of the spectra within each detector and the time relationships between events in the module as well as the influence of the CRUMB anticoincidence veto upon these signals.

Energy calibrations were obtained for both detectors. A spectrum obtained with a gamma ray source irradiating the outer detector is displayed in Figure 7. An inner detector spectrum obtained with the same source is shown in Figure 8. A series of such spectra accumulated in each detector allowed energy calibration of the system and the subsequent adjustment of discriminator windows around the energy regions of the event signature.

Data were obtained concerning the time relationship between pulses in the two detectors. The experimental scheme causes a pulse from the inner detector which is coincident in both photomultiplier tubes which view the scintillator and which is within the proton energy window to start the time-to-amplitude converter (TAC). An outer detector pulse which is coincident in both photomultiplier tubes which view that scintillator and which is within the neutron energy window will stop the TAC. The results of a time delay spectrum collected in this manner are displayed as the top curve in Figure 9. Neither the cosmic ray anticoincidence nor the prompt rejection criteria were applied for this first experiment. The prompt dwarfs other portions of the spectrum, just as in the similar NaI detector experiment reported in NR4-A.

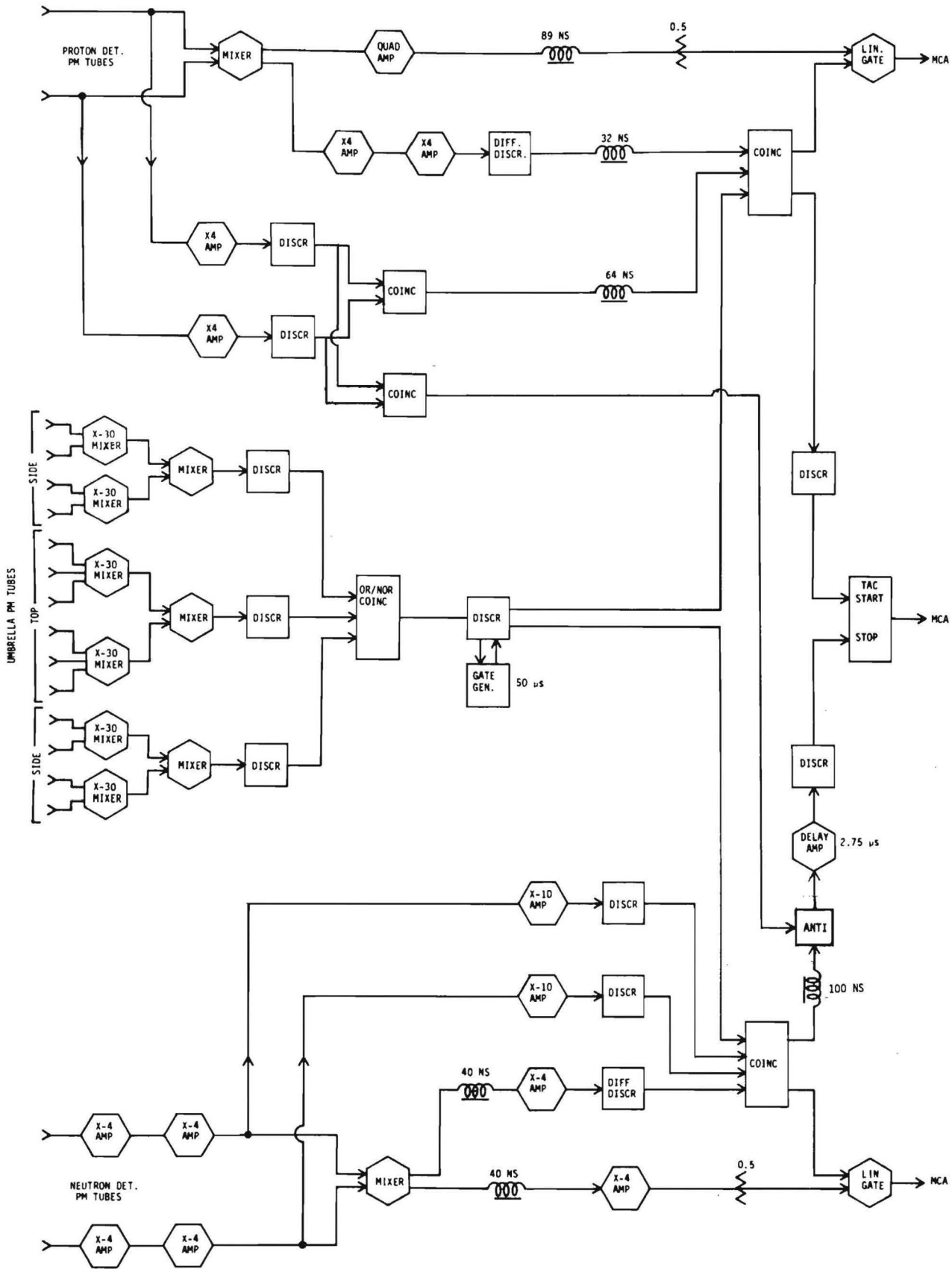

FIGURE 6. SCHEMATIC OF PROTOTYPE MODULE EXPERIMENTAL ELECTRONICS

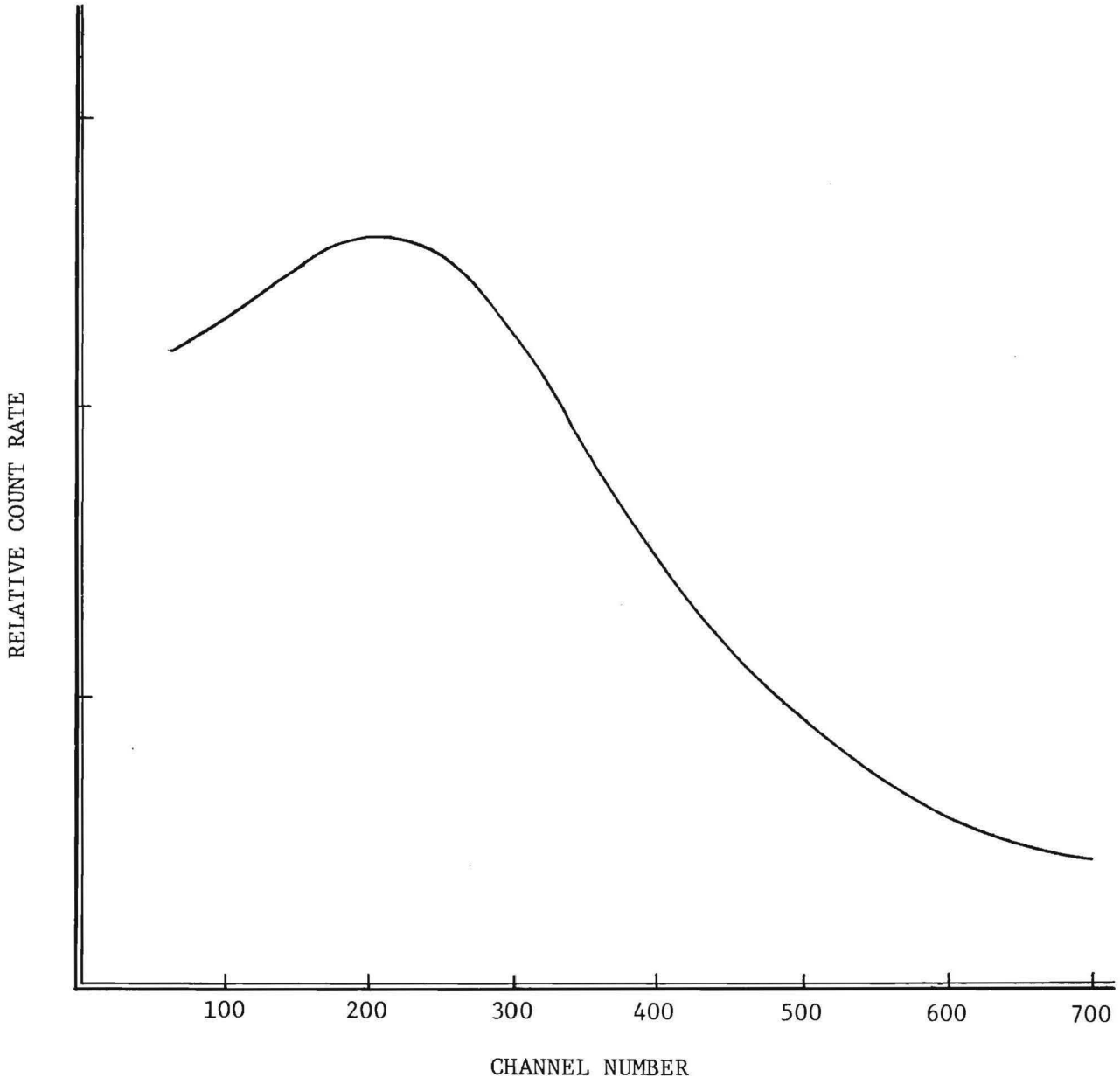

FIGURE 7. OUTER (NEUTRON) DETECTOR RESPONSE TO 0.84 MeV ^{54}Mn DECAY GAMMA RAY.

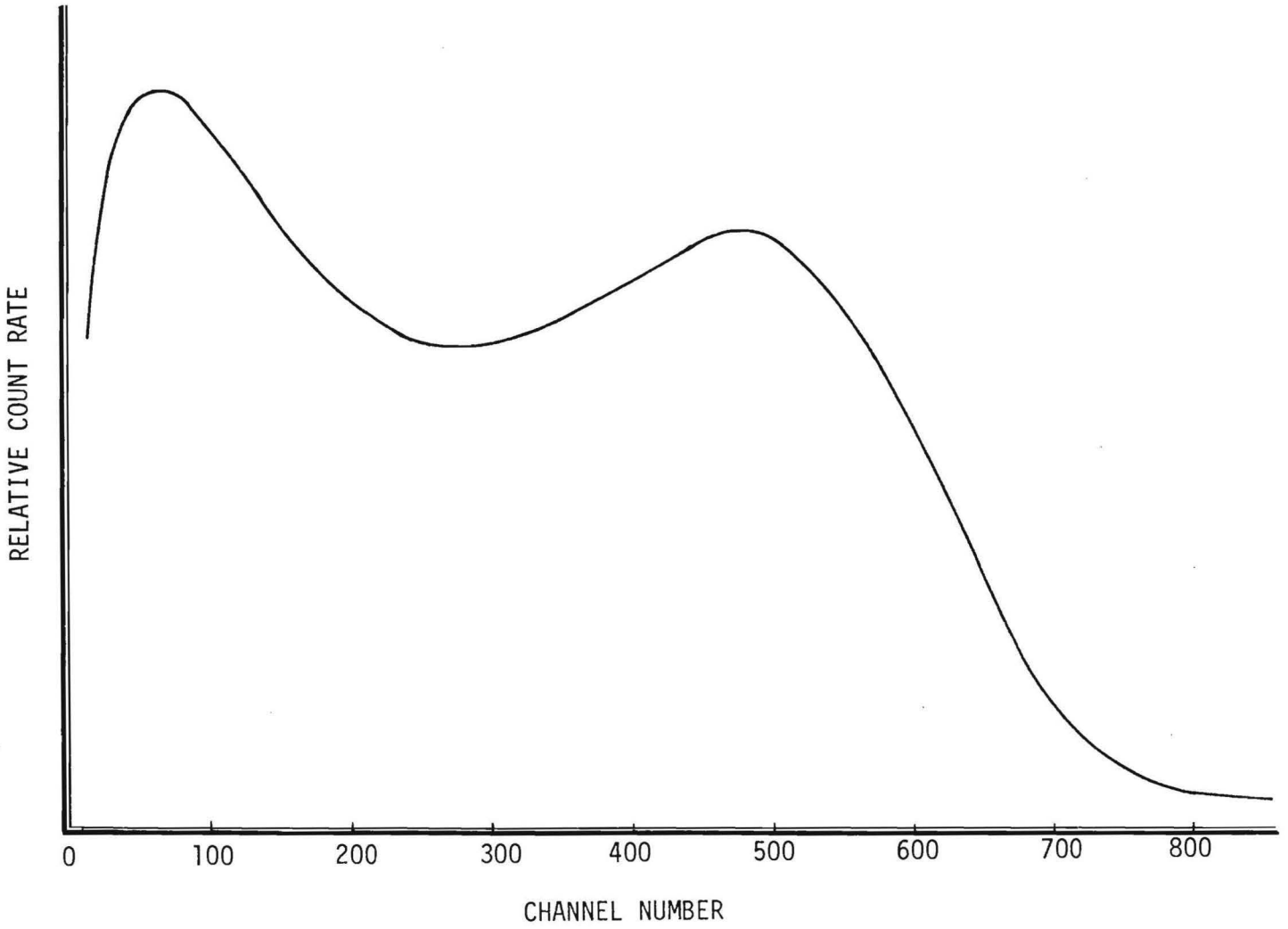

FIGURE 8. INNER (PROTON) DETECTOR RESPONSE TO 0.84 MeV ^{54}Mn DECAY GAMMA RAY

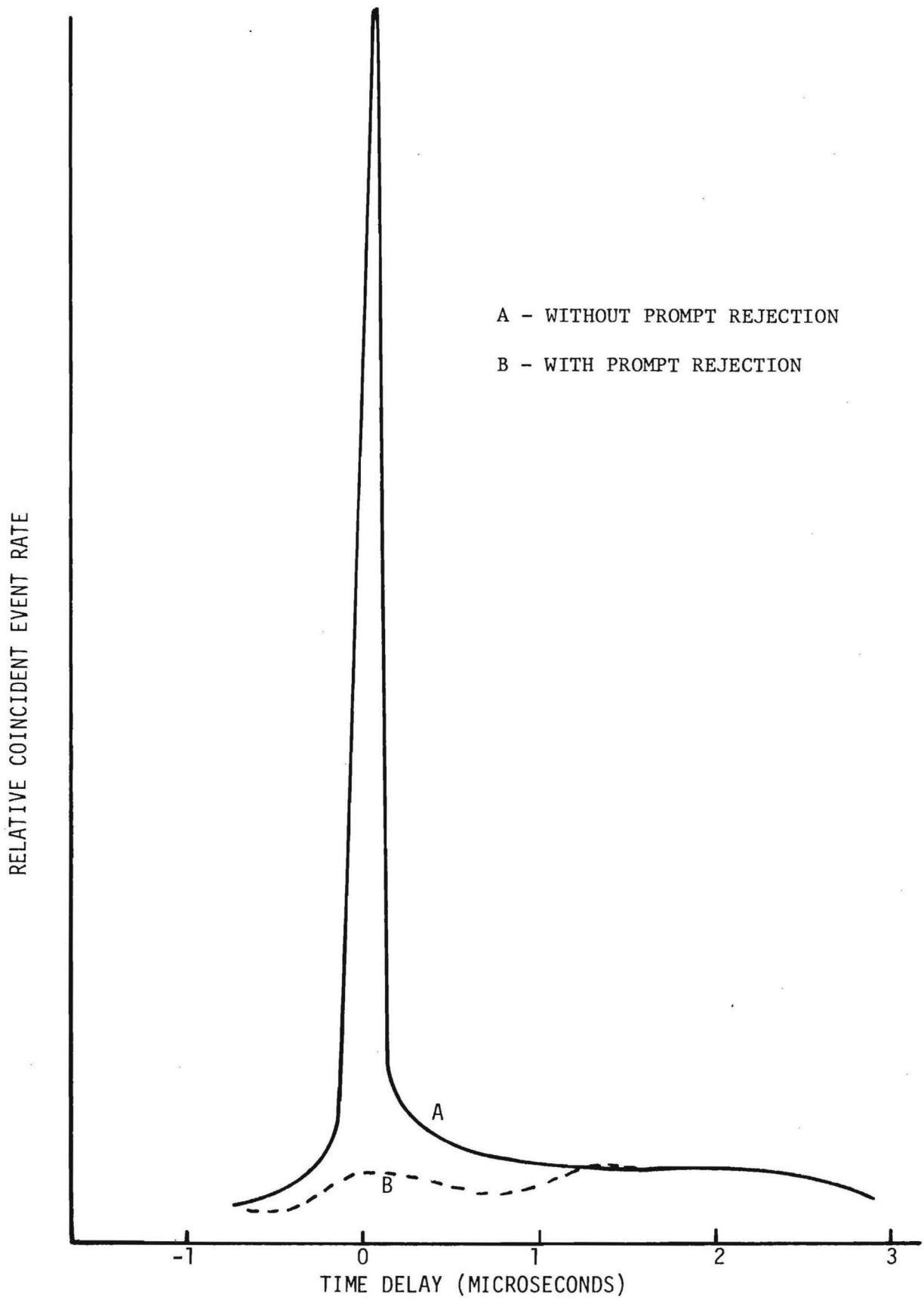

FIGURE 9. PROTOTYPE MODULE TIME DELAY SPECTRA: EFFECT OF PROMPT REJECTION

The effects of the rejection of prompt coincidence events and the cosmic ray anticoincidence upon the time relationship were investigated. The lower curve of Figure 9 shows the effect upon the prompt peak of the rejection of prompt coincidence events (those within 100 nanoseconds). The prompt peak is reduced by a factor of about 20. No CRUMB veto was applied.

Note that the experimental arrangement allowed only rejection of events in the outer detector which are promptly coincident with events within the inner detector. The rejection of inner detector events which are promptly coincident with outer detector events was not applied. The rejection of events of this second sort, as will be instituted during the actual antineutrino-deuteron experiment, will further reduce the observed background signature event rates.

The introduction of both 50 and 500 microsecond wide CRUMB anticoincidence vetoes as well as the restricted prompt rejection requirement allowed the collection of the delay spectra shown in Figure 10. The data have been corrected for the dead time introduced by the veto. The live time rates within the 0.1 to 33 microsecond signature event coincidence time window are displayed in Table 3.

Background Signature Event Rates

As discussed above, the background signature event rates in one module may be expressed as a sum $b_1 + b_2 + b_3$, where b_1 is the rate of correlated events which produce event signatures, b_2 is the rate of correlated events which synthesize the event signature, and b_3 is the rate of chance synthesis. Since the target scintillator of this prototype was undeuterated, b_1 is identically zero. The measured rates in Table 3 are each sums of b_2 and b_3 obtained under various experimental conditions.

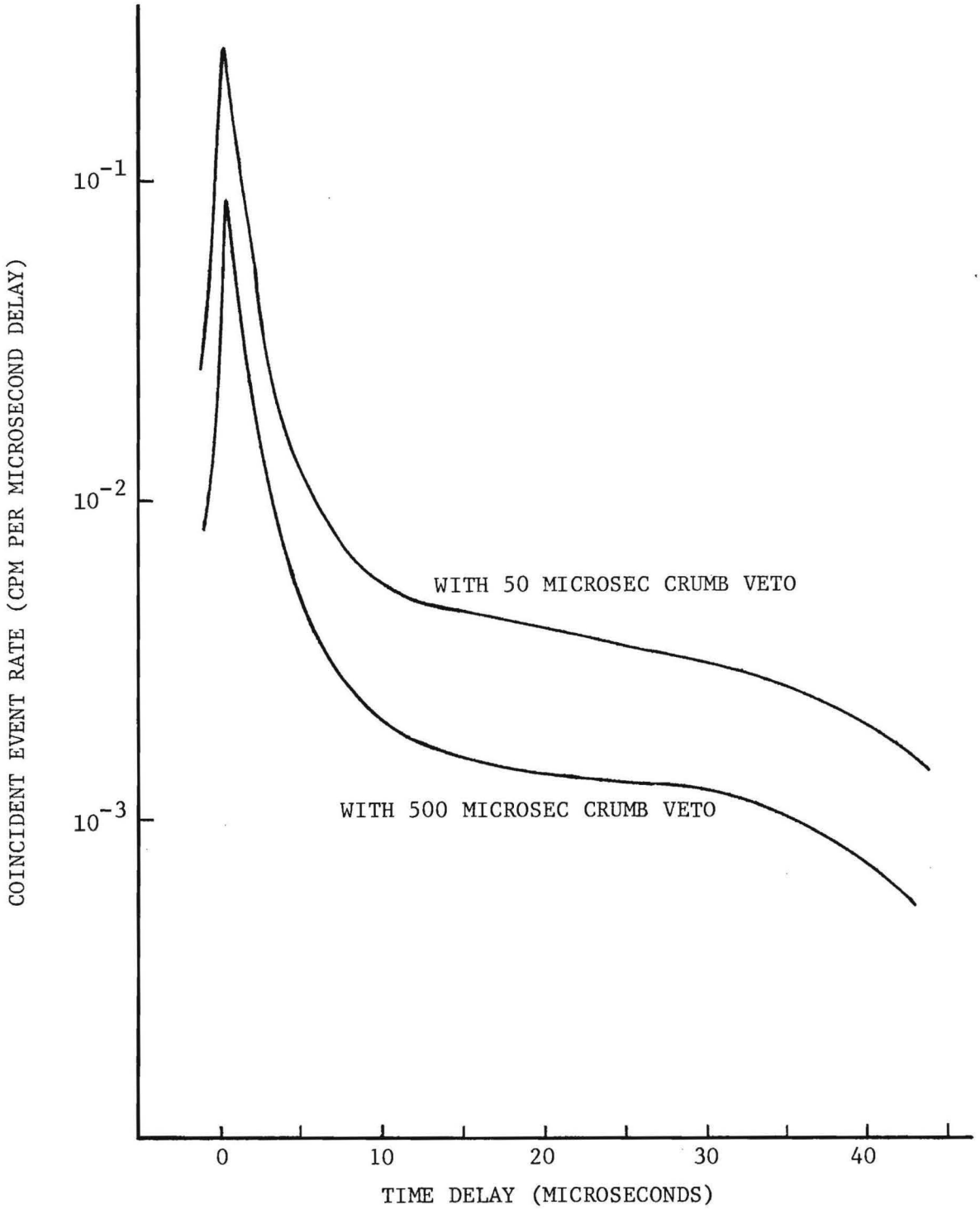

FIGURE 10. PROTOTYPE MODULE TIME DELAY SPECTRUM

TABLE 3

BACKGROUND SIGNATURE EVENT RATES OF PROTOTYPE

(With Rejection of Promptly Coincident Outer Detector Events)

	WIDTH OF CRUMB VETO GATE		
	0 microsec	50 microsec	500 microsec
RATE (cpm)	2.32 + 0.05	0.514 + 0.023	0.187 + 0.007

Singles rates within the energy windows were collected for each detector. From these rates, one can calculate the chance synthesis rate b_3. These values are displayed in Table 4.

These calculated rates for b_3 are considerably less than the rate displayed in Table 3, implying that b_2 is the major contributor to the rates. This conclusion is confirmed by the shapes of the time delay spectra displayed in Figure 10, which are not that expected for a random association of inner and outer detector events. We can now display directly the values for b_3 in Table 5.

The signatures which contribute to b_2 arise from events in each detector which are physically correlated in time. There are only two sources for these events, cosmic rays and natural radioactive contaminants. A consideration of these sources will show that the observed rates represent maxima for obtainable rates.

Contributions to b_2 from Radioactive Contaminants

Natural radioactive contamination consists of alpha, beta and gamma sources within the shield. The small penetrating power of alpha and beta radiation reduces their contributions to negligible amounts compared to the gamma rays. A single gamma radiation cannot contribute to b_2 even with the restricted prompt rejection criterion. Two cascade gamma rays are also excluded by the prompt rejection, since life times of nuclear levels are typically much shorter than 100 nanoseconds.

A possible contribution, however, could occur in a decay chain with an intermediate state with a half life of the order of microseconds. Consider, for example, two consecutive beta decays as shown in Figure 11. If $\tau_{\frac{1}{2}}$ were of the order of a microsecond, and γ_1 were detected in the

TABLE 4

CALCULATED CHANCE SIGNATURE RATES (b_3)

	WIDTH OF CRUMB VETO GATE		
	0 microsec	50 microsec	500 microsec
RATE (cpm)	0.031	0.0033	0.0013

TABLE 5

CORRELATED SIGNATURE SYNTHESIS RATES (b_2)

	WIDTH OF CRUMB VETO GATE		
	0 microsec	50 microsec	500 microsec
RATES (cpm)	2.29 ± 0.05	0.511 ± 0.023	0.186 ± 0.007

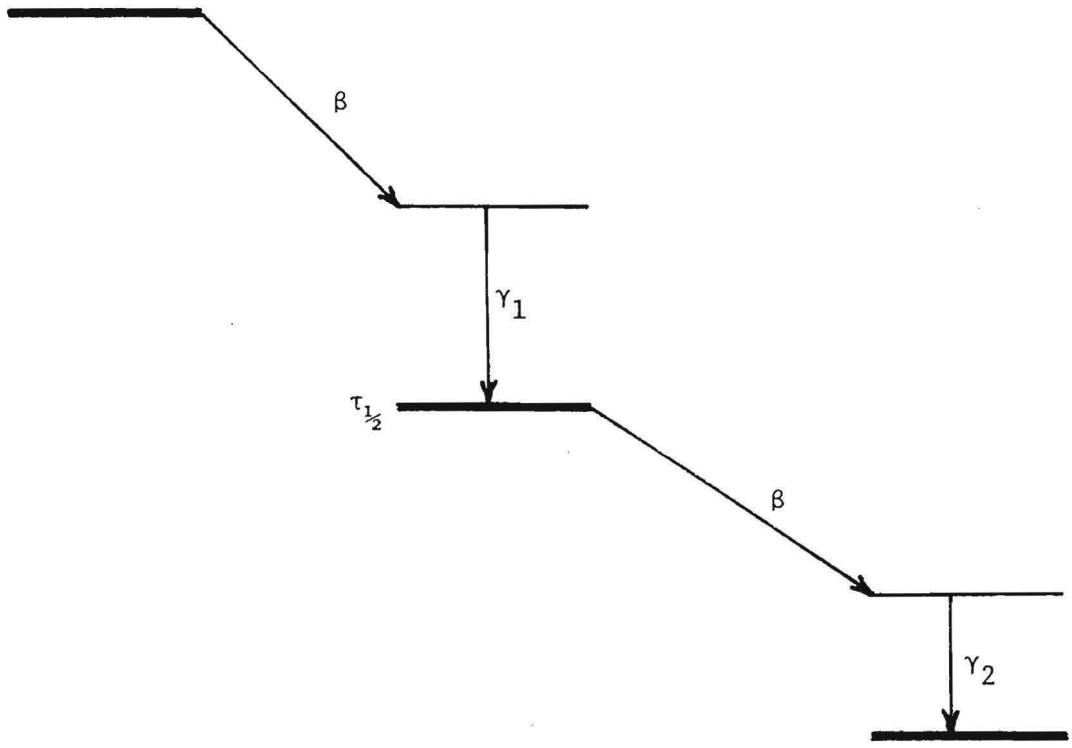

FIGURE 11. GENERALIZED NUCLEAR DECAY SCHEMATIC

inner detector window and γ_2 in the outer detector window, then these events would contribute to b_2. If $\tau_{1/2}$ >> microseconds, these events would appear uncorrelated. If $\tau_{1/2}$ << microseconds, the prompt rejection would remove them.

Consideration of the NaI spectra within the shields indicates the strong presence of the thorium decay chain (see Figure 14). Only ^{212}Po has a half life of the appropriate order, but it cannot contribute signatures to b_2 since it decays to the ground state rather than an excited state of ^{208}Pb, i.e., γ_2 does not exist. A search of the other decay chains produced no appropriate decays.

No candidate for a contributor to b_2 from radioactive contamination can be identified. This strongly implies the conclusion that unvetoed cosmic ray interactions with the shield contribute the bulk of b_2.

Cosmic Ray Contributions to b_2

None of the observed rates are due to the direct passage of cosmic rays through the module. The energy deposited by minimum ionizing radiation passing through both scintillators far exceeds the energy windows. Given the flight times of photons and other swift particles, the effects of cosmic rays upon signature event rates with prompt rejection must be mediated by cosmic ray secondaries created within the shield.

Although the Shield II CRUMB provided good coverage for direct cosmic ray interactions with the module, it covered only about 75% of the bulk material of the shield. Consequently, cosmic ray interactions in the end portions of the shield contribute directly to the unvetoed secondary neutron flux which diffuses through the shield.

The available data allow an estimate of this effect. The rate b_2 can be expressed as a sum

$$b_2 = b_2(D) + b_2(U) \ , \tag{4}$$

where $b_2(D)$ is due to events caused by cosmic rays which interact with the CRUMB and $b_2(U)$ by the others. One can separate $b_2(D)$ into a sum as well:

$$b_2(D) = b_2(DA) + b_2(DB) + b_2(DC) \ , \tag{5}$$

where $b_2(DA)$ is due to signatures which occur within 50 microseconds of the CRUMB event, $b_2(DB)$ signatures within 50 and 500 microseconds, and $b_2(DC)$ signatures beyond 500 microseconds.

The measured rates of b_2 at 0, 50 and 500 microseconds wide CRUMB veto gates may be expressed as

$$b_2(0) = b_2(U) + b_2(DA) + b_2(DB) + b_2(DC) \tag{6}$$

$$b_2(50) = b_2(U) + b_2(DB) + b_2(DC) \tag{7}$$

$$b_2(500) = b_2(U) + b_2(DC) \ . \tag{8}$$

These directly imply

$$b_2(DA) = b_2(0) - b_2(50) = 1.78 \text{ cpm} \tag{9}$$

$$b_2(DB) = b_2(50) - b_2(500) = 0.325 \text{ cpm} \tag{10}$$

where values for measured b_2 rates are taken from Table 5.

It should be noted here that the directional component of the cosmic ray secondaries is contained in $b_2(DA)$ and not in $b_2(DB)$. Charged particle or photon secondaries must interact or decay before 50 microseconds, and neutron secondaries should suffer sufficient collisions before 50 microseconds to become diffuse. The rate $b_2(DB)$ must basically contain only events mediated by the diffuse neutron flux.

The rate $b_2(U)$ can be expressed as the sum

$$b_2(U) = b_2(UA) + b_2(UB) + b_2(UC) \ , \qquad (11)$$

where the terms are defined comparably to those of equation (5).

As noted above, $b_2(DA)$ includes events derived from directional cosmic ray secondaries. The contribution of directional cosmic ray secondaries to $b_2(UA)$ must be considerably reduced. The top and both sides of the module were completely shielded by the CRUMB, which extended as well for two feet beyond the ends of the sensitive volume of the module. Given the $\cos^2\theta$ distribution of the cosmic ray flux, directional events must provide a severely reduced portion of $b_2(UA)$. However, since the fraction of events attributable to directional cosmic ray secondaries is unknown for both $b_2(UA)$ and $b_2(DA)$, an estimate of the effect of extending the shield coverage cannot be made for events within 50 microseconds of detection of a cosmic ray in the extended CRUMB.

The rates $b_2(UB)$ and $b_2(DB)$ do not suffer these difficulties. Hence,

$$b_2(UB) = 1/3\ b_2(DB) = 0.108 \text{ cpm} \ . \qquad (12)$$

We conclude that $b_2(U) \geq 0.108$ cpm, and, much more importantly, additional coverage of the shield by the CRUMB would allow the elimination of at least 0.108 cpm from $b_2(500)$.

Another feature of these data which inflates them over obtainable minima was the lack of an updating discriminator for the CRUMB anticoincidence veto pulse. For long pulse widths, the coincidence of two CRUMB anticoincidence pulses should produce an extended anticoincidence pulse for correct veto of cosmic ray secondary induced pulses. These data were collected without such an extension, and consequently include cosmic ray related events which could be eliminated.

The rate of CRUMB events which fall within 500 microseconds of a previous CRUMB event is random and is given by

$$r_c = 500 \times 10^{-6} \times (5 \times 10^2)^2 = 125 \text{ sec}^{-1} \qquad (13)$$

for our CRUMB event rate of 500 sec^{-1}, or 25% of the CRUMB events were improperly vetoed.

It is possible to estimate the effect of the introduction of an updating CRUMB veto. The difference between the observed rates at 50 and 500 microsecond wide CRUMB vetoes can only be due to cosmic ray secondaries. We will make the naive assumptions that none of the 500 microsecond rate is due to unvetoed cosmic ray secondaries from CRUMB events preceeding the signature by at least 500 microseconds, and that signatures caused by cosmic ray secondaries are distributed uniformly between 50 and 500 microseconds after a cosmic ray interaction with the shield.

The effect upon the signature rate of CRUMB events which occur during a previously begun veto pulse is then given by 25% of $(b_2(50) - b_2(500)) \times \frac{1}{2}$ = 0.041 cpm. But now the appropriate $b_2(500)$ is 0.145 cpm. Iterating this algorithm until the rate no longer decreases in the third significant digit, the expected reduction is 0.046 cpm.

The results of these analyses are summarized below:

a. $b_3 << b_2$

b. The use of an updating CRUMB discriminator alone would reduce $b_2(500)$ by 0.046 cpm.

c. Extension of the CRUMB would reduce $b_2(500)$ by 0.108 cpm.

Shield III

The restrictions of Shield II prevented the insertion of the stainless steel prototype and the location within a deep well also restricted

access to the module. An expanded shield, Shield III, was constructed within a floor level light tight room. It is shown in Figure 12 in schematic cross section. A total of 10 inches of lead surrounds the detectors in all directions. This bulk shielding serves to protect the detectors from the low energy component of the cosmic rays as well as from the natural radiation of the environmental contaminants. The two thicknesses of borated polyethylene provide four inches of neutron protection completely surrounding the detectors. The total mass of the shield is 30 tons.

The cosmic ray umbrella (CRUMB) consists of nine distinct detectors which serve to protect the module from the effects of the high energy component of the cosmic rays when operated in anticoincidence with the module. One hundred gallons of mineral oil scintillator and two slabs of plastic scintillator form the sensitive volumes of the CRUMB. The signals from the 27 photomultiplier tubes are processed to produce an anticoincidence gate pulse when high energy, minimum ionizing radiation interacts with any of the detectors. The photograph in Figure 13 shows some of the details of the shield and CRUMB.

The efficacy of the shield is demonstrated by the spectra obtained with a 3 inch by 3 inch NaI(Tl) detector viewed through an 8 inch long light pipe. These spectra are displayed in Figure 14. The topmost curve shows the data obtained with the detector outside the shield. The peaks are associated with known gamma ray transitions of natural radioactive contaminants of the environment. The second spectrum, obtained with the detector inside the shield, demonstrates a general two orders of magnitude reduction in the spectrum. The remaining continuum is largely associated with the cosmic rays, as is demonstrated by the third curve which displays

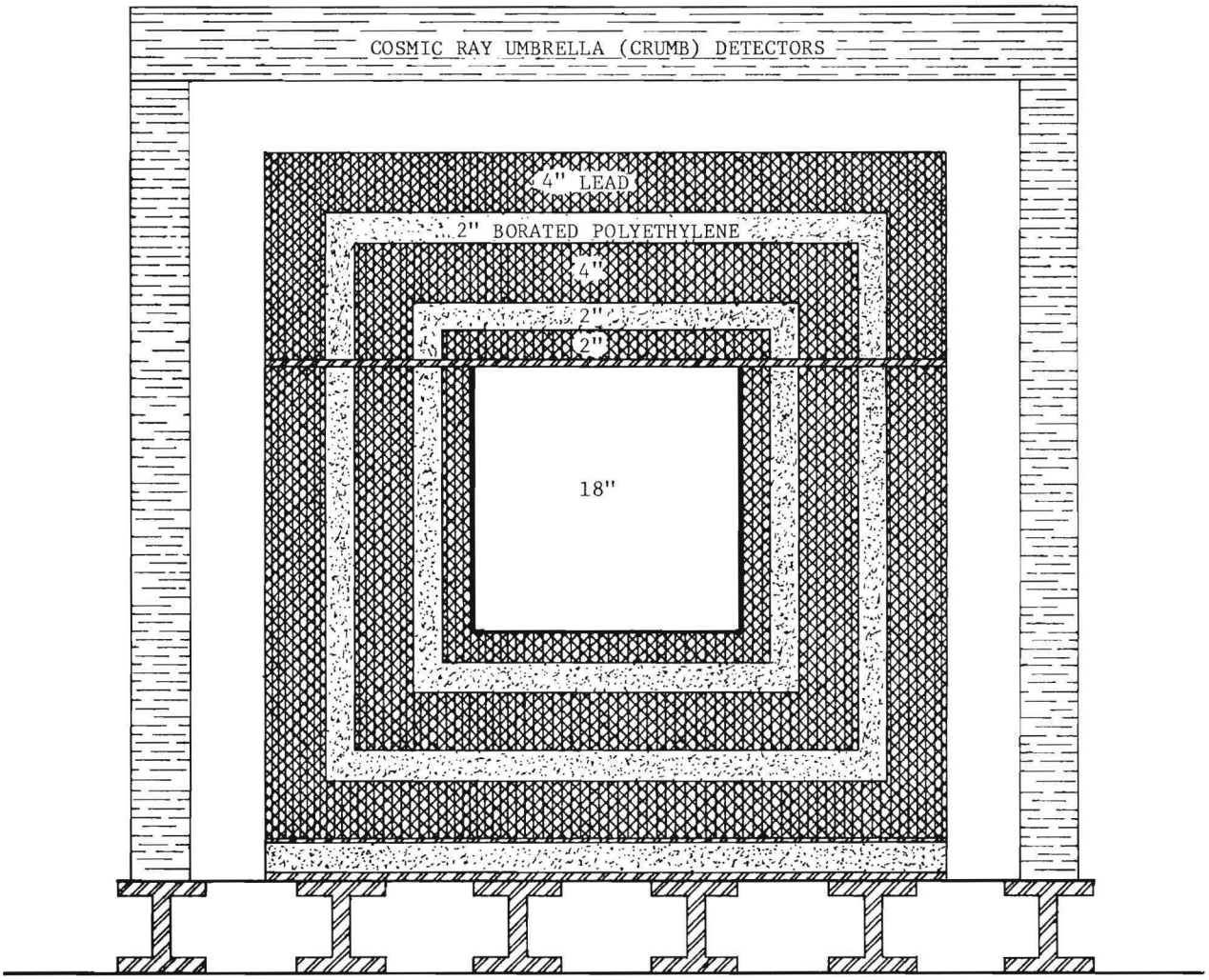

FIGURE 12. CROSS SECTION DRAWING OF SHIELD III

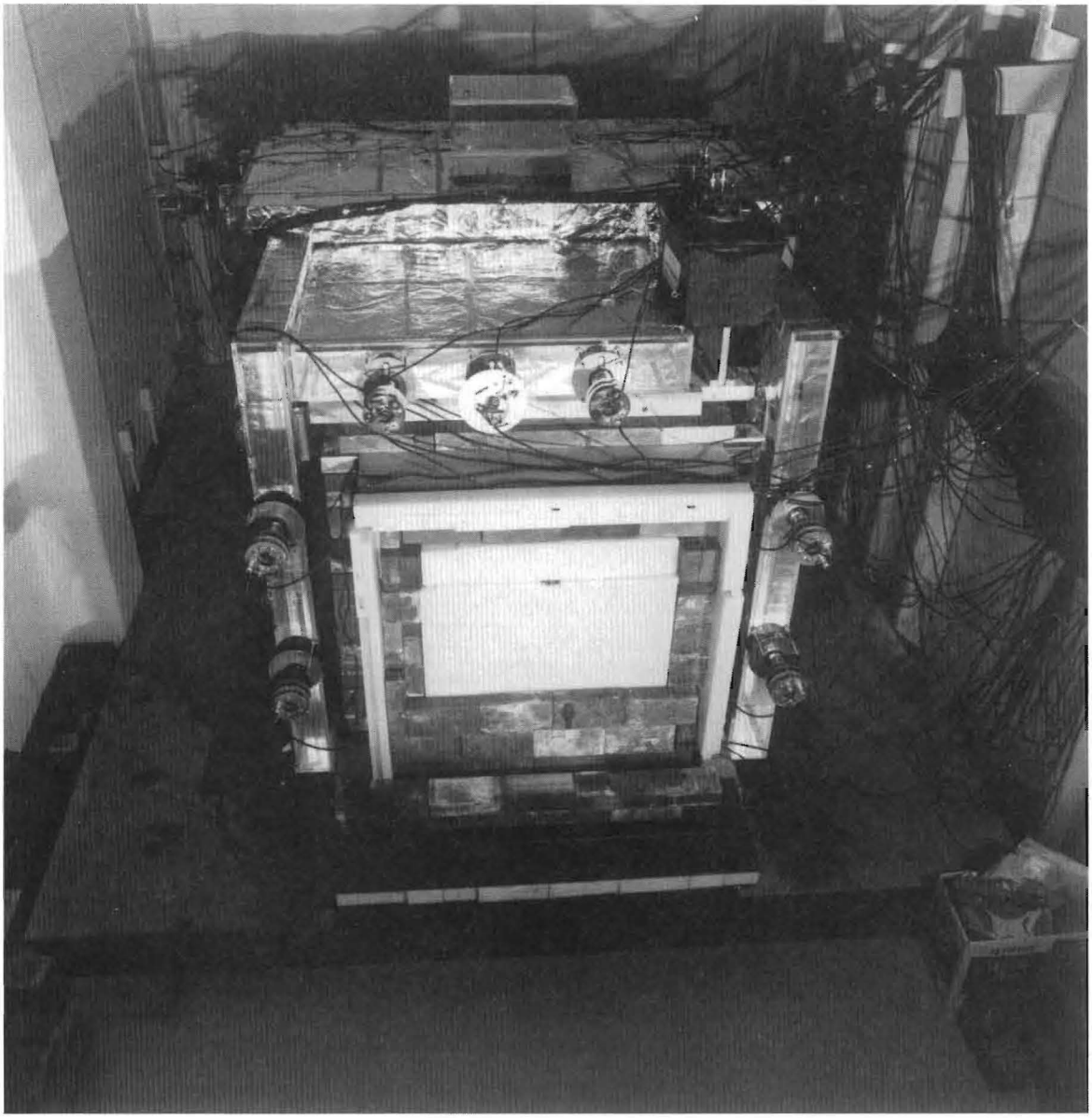

FIGURE 13. COSMIC RAY UMBRELLA DETECTORS AND BULK SHIELD III

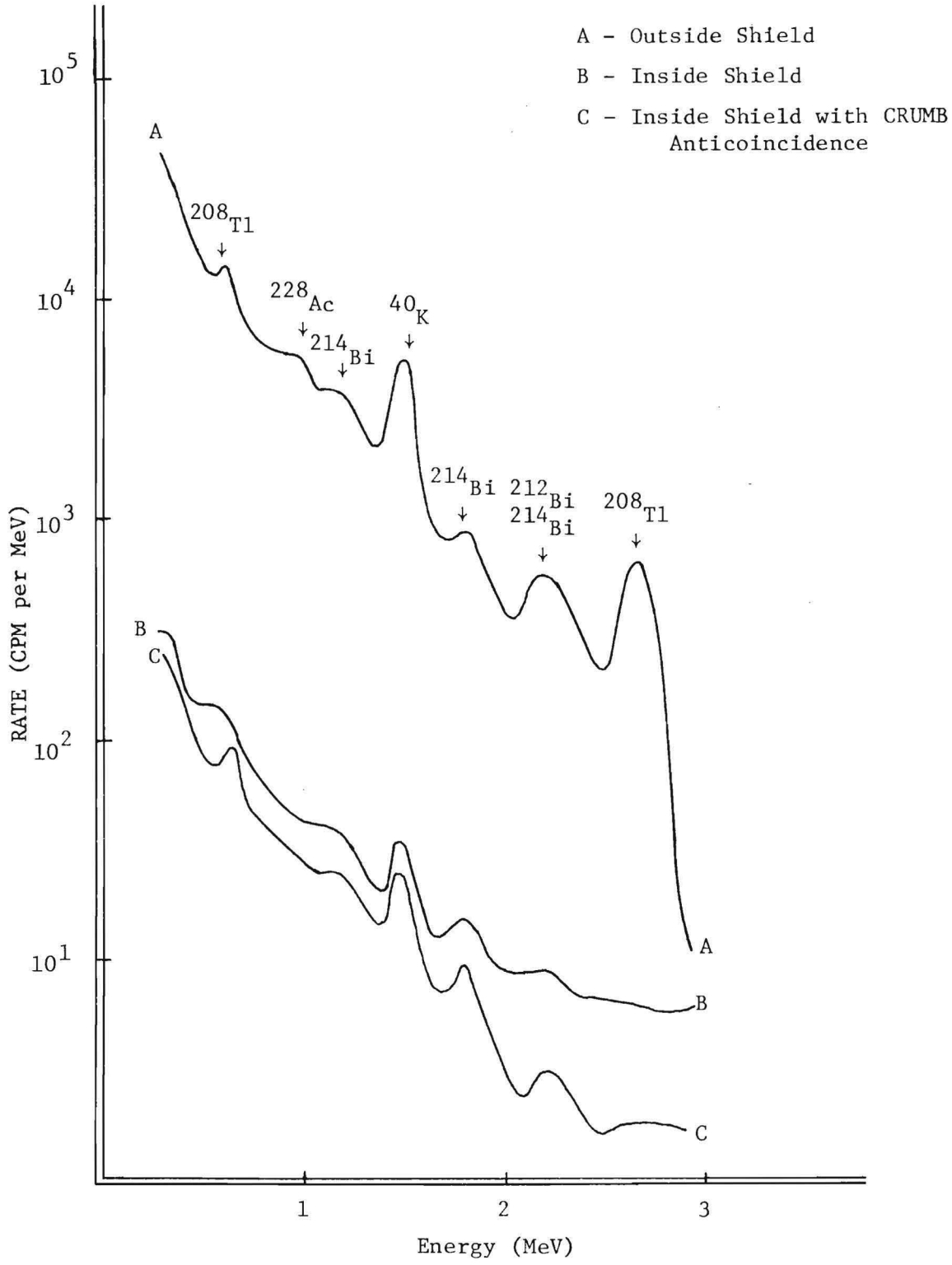

FIGURE 14. SURVEYS OF SHIELD WITH A SODIUM IODIDE DETECTOR

data obtained with the detector inside the shield and in anticoincidence with the CRUMB. The factor of two reduction in the continuum accentuates the peaks, as one would expect of radiations unassociated with the cosmic rays. The reduction was obtained with a four microsecond long anticoincidence gate. Experiments with previous shields have demonstrated the usefulness of longer anticoincidence gates, which will be required for the experiment.

Stainless Steel Prototype Detector Module

It had been decided earlier that two modules would be built, one of stainless steel with quartz windows and a clear teflon reflector and the other of acrylic, very similar to that used in the background measurements. The reason that the stainless steel cell was designed and planned at all was that earlier attempts to contain the ^{6}Li-butoxide scintillator in acrylic had resulted in rapid deterioration of the scintillator. It was thought that moisture and oxygen either trapped on the surface or diffusing through the acrylic was the cause of the deterioration.

The transfer system shown in Figure 15 was assembled and it was decided that the stainless steel module would be filled first. This decision was made for two reasons: first, funds for the production of more of the ^{6}Li-butoxide loaded scintillator than what was on hand at the beginning of the project were removed from the grant request and only enough scintillator was on hand to fill one cell and second, it had been demonstrated many times earlier that the scintillator could be successfully contained in stainless steel cells with teflon seals. It was also considered highly important to demonstrate that the delicate lithium loaded scintillator could be transferred successfully without degradation

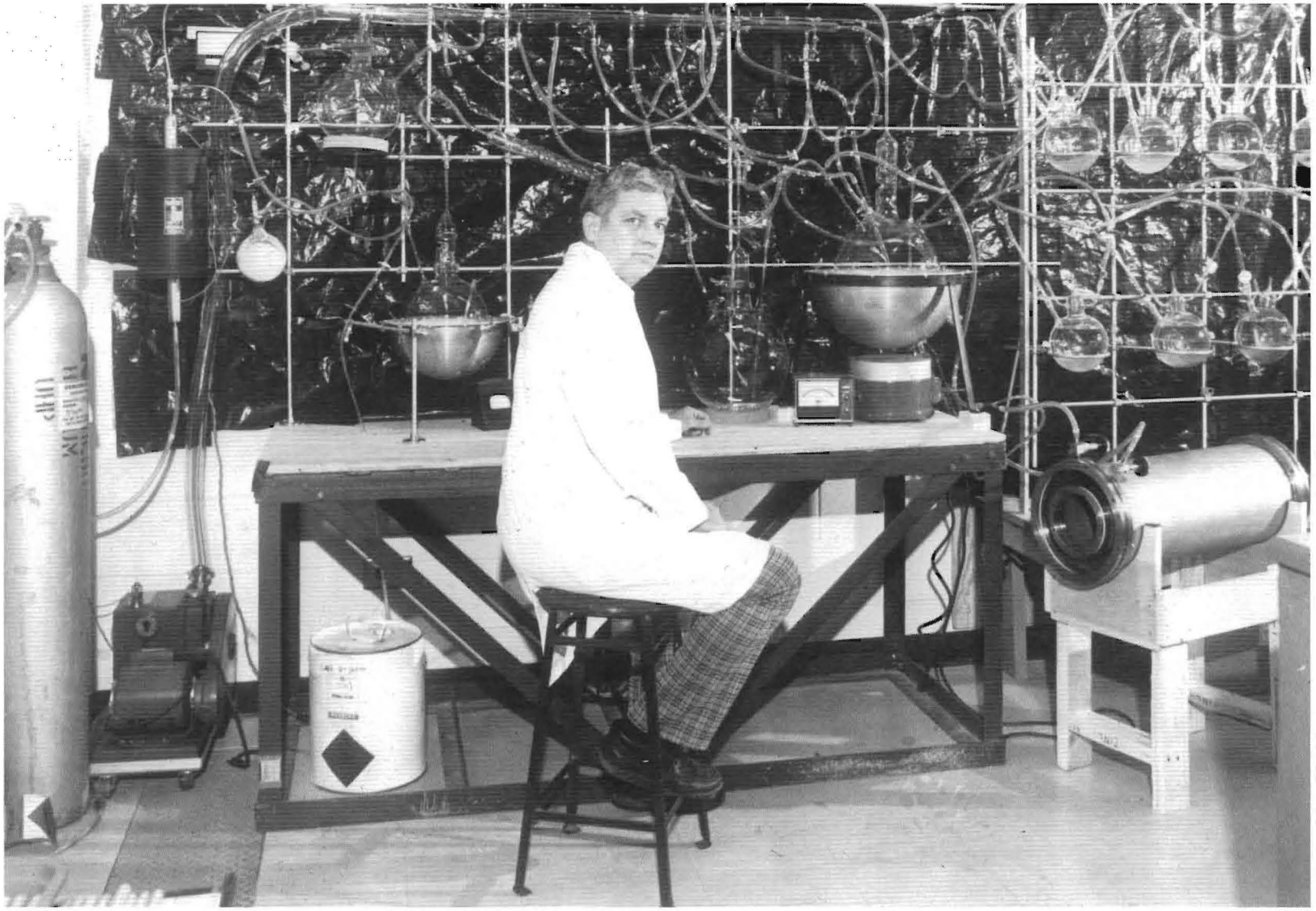

FIGURE 15. SYSTEM FOR MIXING AND TRANSFERRING LITHIUM LOADED SCINTILLATOR

and if the acrylic cell were chosen first and there were some degradation, the cause would not be at all clear.

The steel cell is shown in Figures 16 and 17 and the total assembly with light pipes and 9 inch diameter (60 DVP) Amperex photomultiplier tubes are shown in Figure 17 and again in Figure 18 just prior to installation inside the shield. The control console containing the electronic systems supporting the dual module and live shield are shown in Figure 19.

The first transfer of the scintillator was successful and no degradation of the scintillator was noted. A small sample of the scintillator was transferred at the same time to a small glass cell and its scintillation properties were observed and found to be very similar to those of earlier tests. The scintillator was contained within the cell for one week and no sign of degradation was observed, demonstrating again that these materials are compatible with lithium butoxide. After this successfull demonstration, the scintillator was transferred back into the transfer system and the cell was cleaned and prepared for filling again. Prior to the second transfer, one of the quartz windows was accidentally broken. At this point it was decided that rather than to suffer the delay of obtaining a new window it would be expedient to try an acrylic window instead. This was considered acceptable since prior experience demonstrated that several days was required for the scintillator to deteriorate and it would be possible to test the cell before significant degradation. This could also determine whether the acrylic itself was responsible for the deterioration of the scintillator in earlier tests of whether possibly the method of sealing the joints with acrylic glue was responsible. The lithium loaded scintillator was again successfully transferred into the cell and was observed for almost ten months. No degradation of the

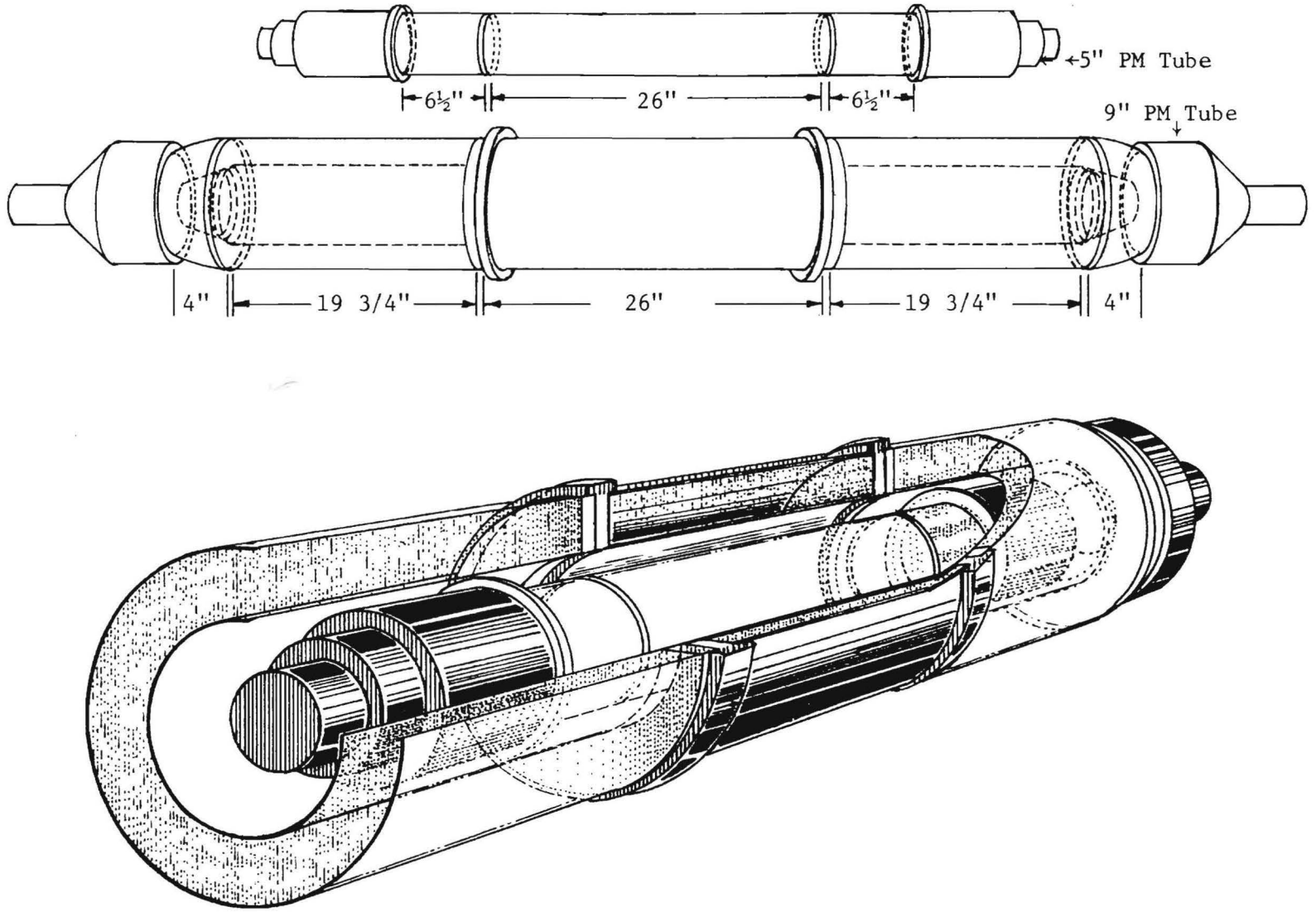

FIGURE 16. SCHEMATIC OF DUAL CONCENTRIC PROTOTYPE DETECTOR MODULE (STAINLESS STEEL VERSION)

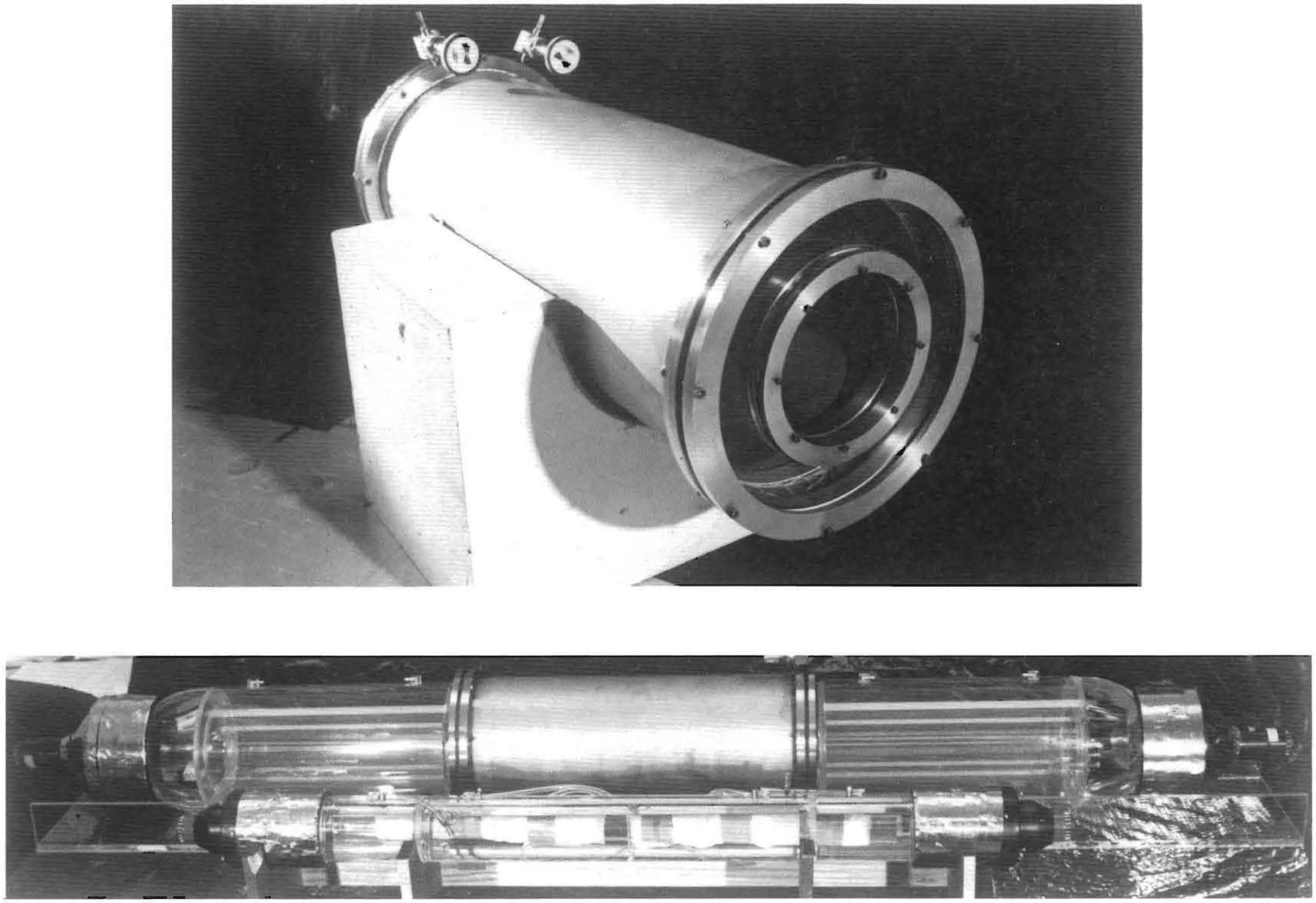

FIGURE 17. DUAL CONCENTRIC PROTOTYPE DETECTOR MODULE (STAINLESS STEEL VERSION) SHOWING SEPARATE COMPONENTS

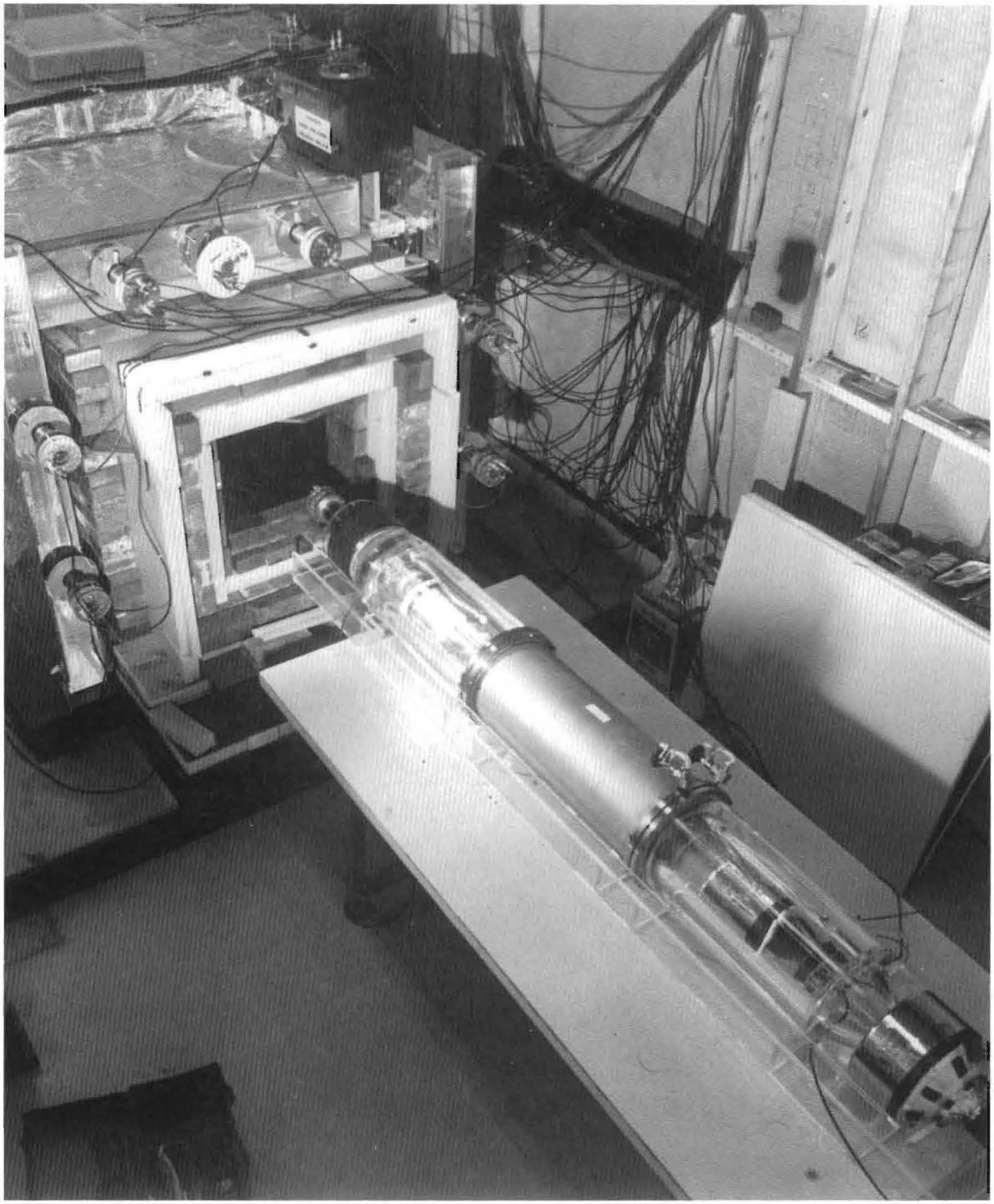

FIGURE 18. ASSEMBLED DETECTOR MODULE READY FOR INSERTION INTO SHIELD III

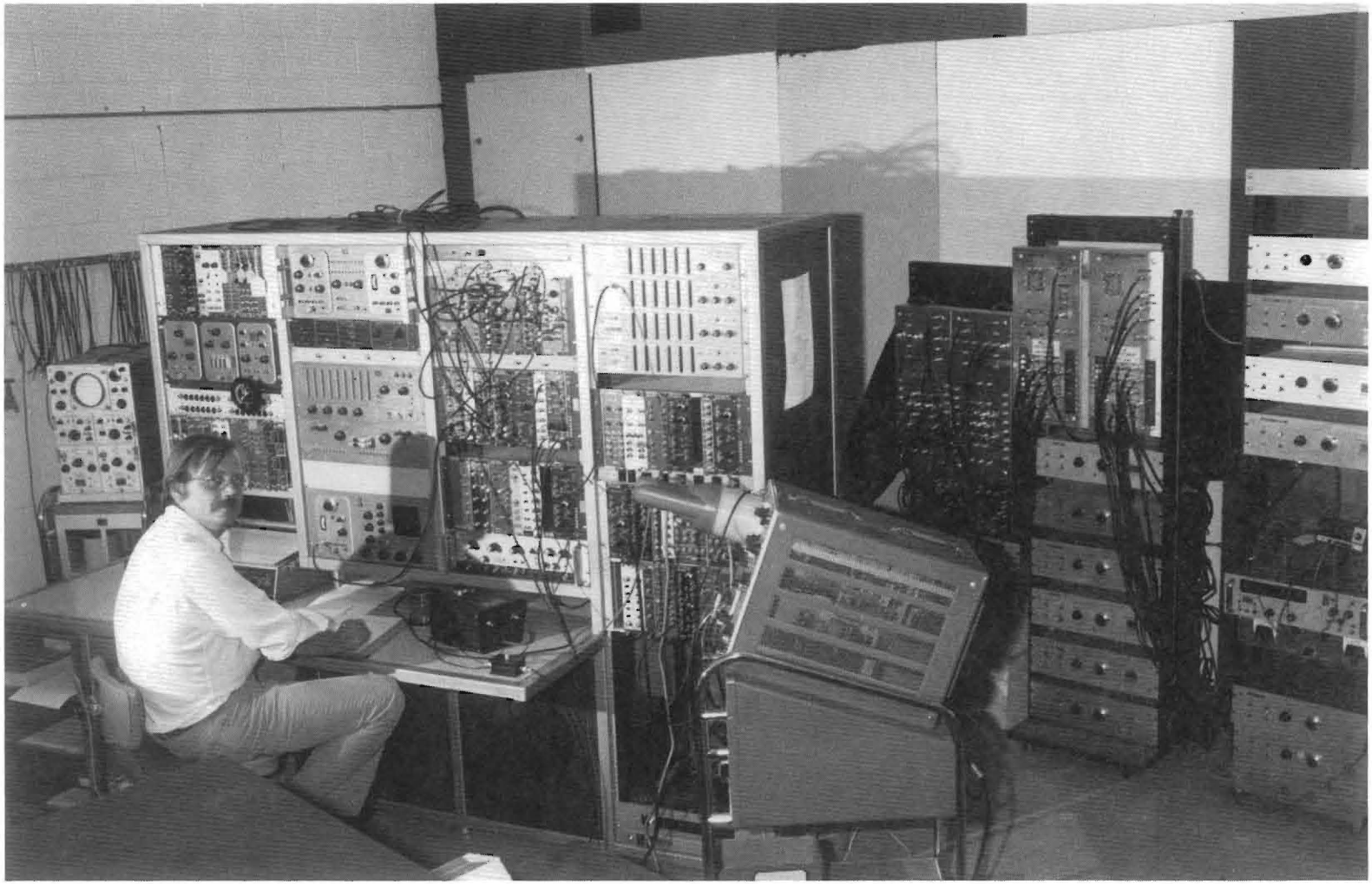

FIGURE 19. SAM BLANKENSHIP SEATED AT THE ELECTRONICS CONSOLE

scintillator was observed. Hence, it is now clear that an acrylic cell with "O"-ring joints can be used to construct the outer cell. This conclusion has led to a significant simplification of the development phase of the project because the light collection properties of an acrylic cell of the required geometry and size were thoroughly investigated in the feasibility study of the acrylic prototype module. We have had the opportunity to study the light collection properties of the stainless steel cell lined with clear teflon and we find that the acrylic cells have significantly better light collection properties than that of the steel cell. In addition, the acrylic cells we have already tested definitely have light collection properties which are more than adequate to perform the proposed experiment.

Experimental Work in Progress

The experimental simplifications inherent in a smaller number of larger modules was discussed in NR4-A, the previous progress report. To examine the relative merits of a larger central cell, a prototype eight-inch diameter central cell was constructed of acrylic. (See Figure 20.) With such an inner detector, two modules would be sufficient to contain 40 liters of target scintillator.

The central portion of the cell was filled with mineral oil based scintillator and the light pipes with pure mineral oil. Amperex 60DVP nine-inch diameter photomultiplier tubes were coupled to each end.

The cell was irradiated with gamma ray sources. A typical spectrum is shown in Figure 21. The association of energies with spectral characteristics was more complicated than that of the five-inch cells. The effects of more common multiple Compton events washes out many features from low energy gamma

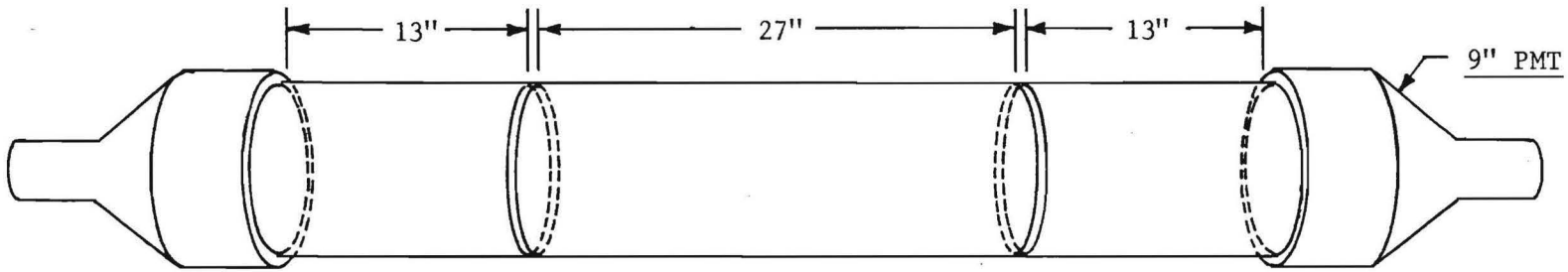

FIGURE 20. DETAILS OF 8 INCH INNER DETECTOR PROTOTYPE

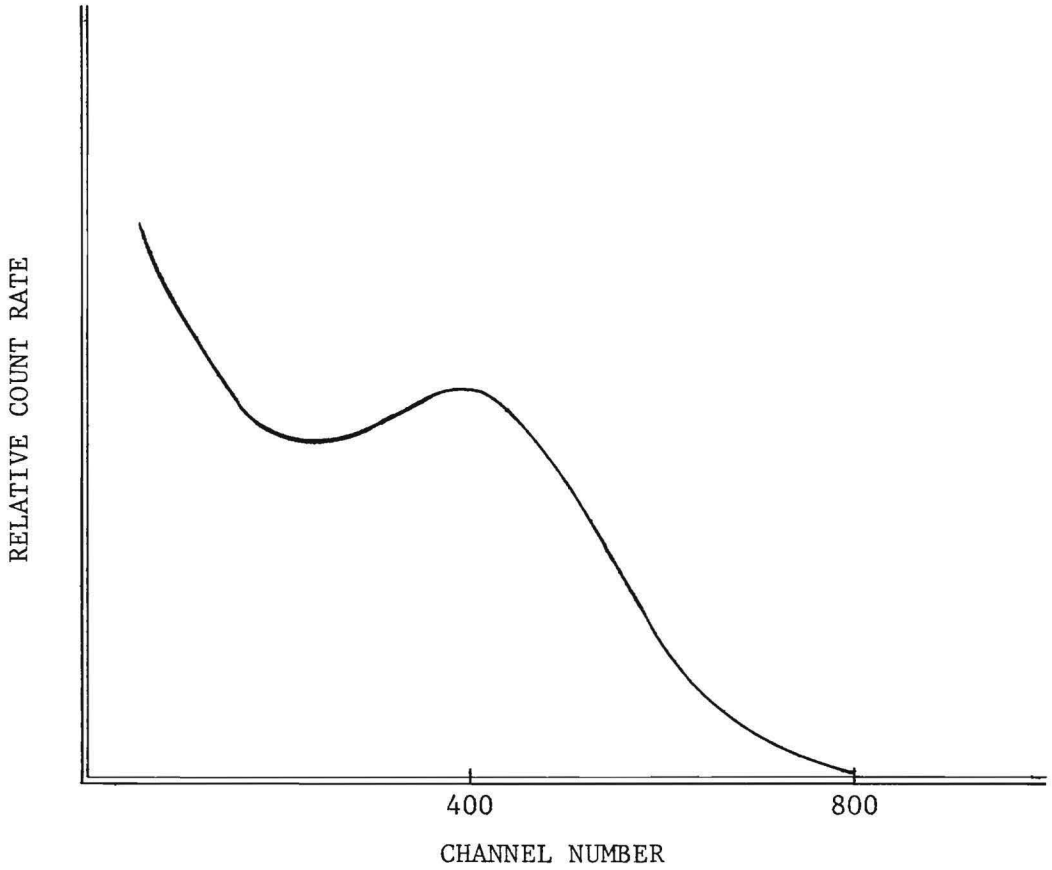

FIGURE 21. 8 INCH INNER DETECTOR PROTOTYPE RESPONSE TO ^{137}Cs GAMMA RAYS

ray spectra, which complicates the selection of the appropriate resolution function. While this work progressed, a preliminary energy calibration was obtained.

Spectra were collected with the cell contained in Shield III, with and without CRUMB coincidence and veto gates. These are displayed in Figure 22 as a function of the preliminary energy calibration. These spectra may be compared to those obtained in the five-inch cell shown in Figure 16, page 41 of NR4-A. The spectra have similar features, although the differences in widths of CRUMB gates preclude direct comparison.

Work is continuing to achieve a precise energy calibration and to investigate other parameters such as uniformity of response. These results will permit a comparison of the two cell sizes.

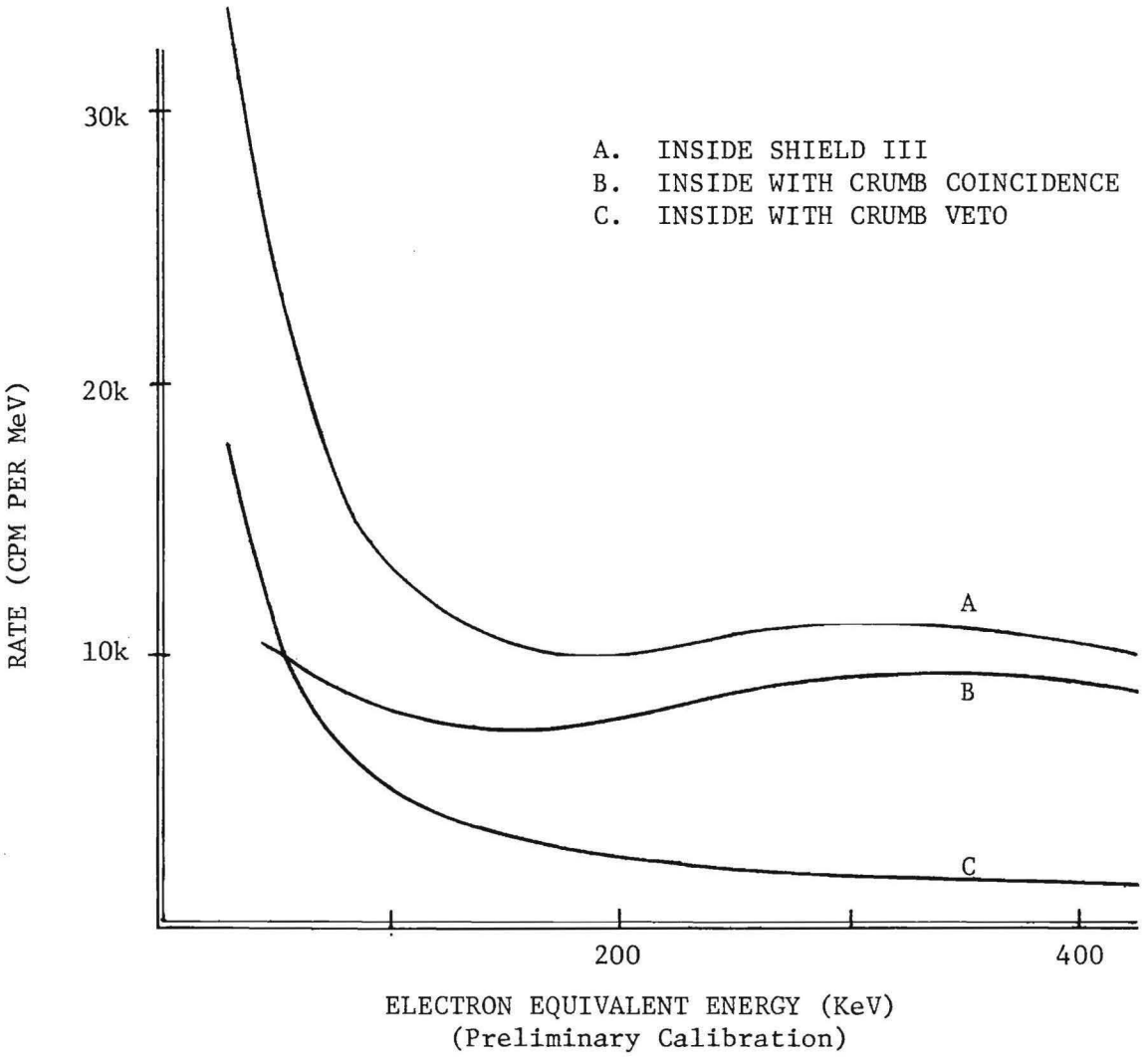

FIGURE 22. PULSE HEIGHT SPECTRA OF BACKGROUND IN 8 INCH INNER DETECTOR PROTOTYPE

Chapter 4

CONCLUSIONS

The data obtained to date and described in the preceeding sections and in NR4-A lead to some positive conclusions about the feasibility of the proposed experiment. All aspects of the experiment design have now been investigated to some degree. The data are adequate to demonstrate feasibility.

The event rate to be determined from the experiment is that of the reaction (1). For this experiment, it has the predicted value of 2.1 per hour.

$$I_o = \phi_{\bar{\nu}_e} \sigma_{\bar{\nu}d} N = 2.1 \text{ per hour} = 49.5 \text{ per day} , \qquad (14)$$

where:

$$\phi_{\bar{\nu}_e} = 3 \times 10^{13} \text{ cm}^{-2} \text{ sec}^{-1} ,$$

$$\sigma_{\bar{\nu}d} = 7.4 \times 10^{-45} \text{ cm}^2$$

$$N = 2.58 \times 10^{27} \text{ deuterons/40 liters}$$

The actual detected rate, S, due to this reaction will be smaller by a factor determined by the experimental efficiency and the number of reaction products falling within the signature limits.

$$S = k_p \cdot k_n \cdot k_\tau \cdot I_o = 0.97 \text{ per hour} = 23.2 \text{ per day} , \qquad (15)$$

where the fractions k_p, k_n and k_τ are the fractions of the total number of $\bar{\nu}_e$ events which fall within the signature constraints ΔE_p, ΔE_n and $\Delta\tau$. The values are:

$$k_p = 0.58$$

$$k_n = 0.90$$

$$k_\tau = 0.90 \ .$$

The measurement consists of a difference between signature event rates with the antineutrino flux present and not present. Adequate shielding isolates the detectors from the other radiations of the reactor and the experimental arrangement allows discrimination against the other antineutrino induced events. (See NR4-A, Section B.) These precautions alone would allow a measurement of the antineutrino induced deuteron disintegration event rate to any desired precision given sufficient time. The restraints imposed by long term instrumentation instability and the resources of the experimenter require that the time to produce the desired result be reasonable. Consequently, a feasibility analysis should emphasize those parameters which affect the counting time.

The counting time was shown in NR4-A, Section B, to have the form

$$T = 2B(k/S)^2 \ , \tag{16}$$

where B is the background rate and k is the constant specifying the statistical accuracy of the measurement. This now reduces to

$$T = 0.0037k^2B \text{ days} \tag{17}$$

or for k = 4, a reasonable requirement for a statistically significant result,

$$T = 0.059B \text{ days} \ . \tag{18}$$

The total background can be represented as the sum of three components (see Chapter 3). The experimental results include measurements of

$b_2 + b_3$ for various experimental conditions. The rate of photodisintegration events, $I_{\gamma d}$, was calculated (see NR4-A, Section C) and the "observed rate," the most significant term of b_1, was obtained by applying the signature delimiter parameters to the nucleon energy distribution calculated for the photodisintegration process. The values so obtained for B are as follows:

$$b_1 = k_p \cdot k_n \cdot k_\tau \cdot I_{\gamma d} = (0.49)(0.9)(0.9)\ 4.25 = 1.7/\text{hour} = 41/\text{day} . \quad (19)$$

The measured value for $b_2 + b_3$ from Table 5 is

$$b_2 + b_3 = 11.2/\text{hour} = 269/\text{day} . \quad (20)$$

Consequently,

$$b = b_1 + b_2 + b_3 = 310/\text{day} , \quad (21)$$

and for six modules with 40 liters of target

$$B = 6b = 1860/\text{day} . \quad (22)$$

It is now possible to estimate the counting time, T, for the proposed experiment. Substituting the background rate, B, from equation (22) into equation (17) gives

$$T = 6.88k^2 \text{ days} \quad (23)$$

or from equation (18)

$$T = 110 \text{ days} . \quad (24)$$

This value is calculated with none of the readily available reductions in b_2 which are discussed in Chapter 3. The effect of b_2 upon T follows directly from equations (3), (18) and (22) and the relationship is displayed graphically in Figure 23. It is obvious that the reductions in

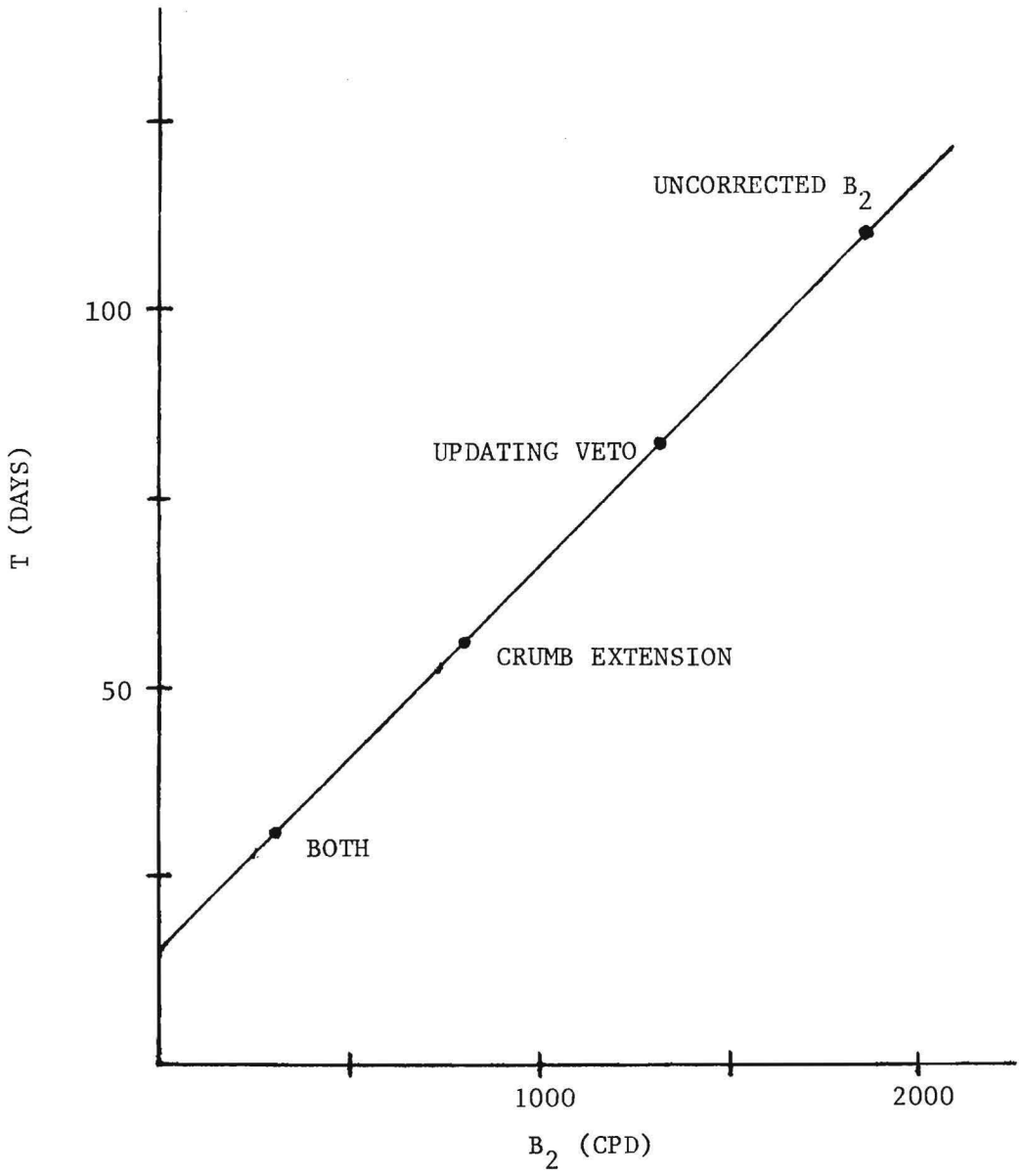

FIGURE 23. COUNTING TIME T AS A FUNCTION OF B_2 (The dots show rates and times for conditions explained in the text.)

b_2 and hence B_2 will provide significant reductions in T.

Simply the introduction of an updating discriminator will reduce b_2 by 2.8/hours; hence

$$b_2 + b_3 = 8.5/\text{hour} = 203/\text{day} , \tag{25}$$

$$B = 6(b_1 + b_2 + b_3) = 1464/\text{day} , \tag{26}$$

and from equation (18)

$$T = 86 \text{ days} . \tag{27}$$

The extension of CRUMB coverage of the shield alone is expected to reduce b_2 by 6.5/hours. By the same arguments

$$T = 55 \text{ days} . \tag{28}$$

The above results display the independent addition of each reduction separately. If both were applied concurrently, as will be accomplished in the experiment, the combined effect is expected to reduce b_2 by 0.154 cpm. This leads directly to

$$T = 31 \text{ days} . \tag{29}$$

This estimate does not include the effect of using an updating CRUMB veto for the extended CRUMB, and thus is an upper limit for T.

It is of great importance to note that these reductions are accomplished by simple hardware additions to the present experimental arrangement and that these additions have always been planned for the actual cross section measurement experiment. Thus there is no impediment to their application nor the resultant reduction in B.

In the actual experiment, an approximately equal amount of time would be required for background subtraction so that the experimental counting time would be 62 days. This counting time does not include the instrumental

dead time. The measured dead time of the apparatus due to the cosmic ray anticoincidence shield, at the present site which has no significant mass above, would imply approximately 50% for full shield coverage. However, this dead time is significantly reduced by a large amount of massive building material above the experiment that attenuates the cosmic ray flux. For a site at the anticipated reactor this reduction is almost an order of magnitude.

There is good justification for viewing this computed value of the counting time as an upper limit to that which will actually be achieved. Several important effects were not included in the data and each can only reduce the value of T. These effects are:

1. Application of prompt rejection of inner detector events by events in the outer detector.

2. Application of prompt rejection for module-to-module scattering. At present the only prompt rejection is that between detectors in a single module.

3. Incorporation of the planned data collection and analysis instrumentation will allow exact optimization of the values for the event signature delimiters. This is not possible with the present instrumentation.

4. Greatly increased overburden at the experiment site compared to the negligible amount at the present site.

It is not unusual for neutrino experiments to consume many months or even years of counting time. The fundamental limitation on the length of counting time is the requirement of maintaining apparatus and instrumentation calibration so that accumulated data may be legitimately integrated. Very careful and detailed consideration has gone into the development of instrumentation and procedures for calibrating and monitoring performance. All of these produce a "coherence" time certainly measured in years. Thus not only is the proposed experiment feasible, but a very high degree of statistical accuracy is possible.

Appendix I

WEAK NEUTRAL DISINTEGRATION OF THE DEUTERON BY REACTOR ANTINEUTRINOS

Weak neutral disintegration of the deuteron by reactor antineutrinos*

F. T. Avignone III and Z. D. Greenwood
Department of Physics and Astronomy, University of South Carolina, Columbia, South Carolina 29208
(Received 28 July 1977)

The spectrum of antineutrinos emitted by beta decaying products of ^{235}U in secular equilibrium has been recalculated using more recent experimental decay-scheme data. The new data involve 26 nuclides with 150 β branches and represent 22% of the total fission yield. The cross section for the reaction $\bar{\nu}_e + d \rightarrow p + n + \bar{\nu}_e$, which proceeds only via the weak neutral current, is shown to be predicted consistently by three theoretical treatments in the literature. The total cross section was calculated by weighting the cross section by the normalized antineutrino spectrum and is 7.4×10^{-45} cm^2.

I. INTRODUCTION

The Lorentz and isospin character of the weak neutral current is of fundamental interest at present mainly because neutral currents are natural consequences of the various gauge theories of weak and electromagnetic interactions (see, for example, Refs. 1–3). There are several experimental examples in which the observation of weak neutral processes were made using high-energy muon neutrinos. A well-known example is the elastic scattering of nucleons via the reaction $p(\nu_\mu,\nu_\mu)p$.[4] The disintegration of the deuteron by electron-antineutrinos via the reaction,

$$\bar{\nu}_e + d \rightarrow n + p + \bar{\nu}_e \,, \tag{1}$$

which can only occur via the weak neutral current was proposed by King and Ahrens, and by Gaponov and Tyutin.[5] Also, total cross sections have been calculated for reactor antineutrinos (see, for example, Ref. 6). Recently the measurement of the cross section for this reaction was experimentally shown to be feasible[7]; hence, the theoretical prediction of the total cross section based on a reliable antineutrino spectrum becomes important.

There are fundamental reasons why the cross section for reaction (1) with low-energy antineutrinos should be carefully measured. The actual quantity determined by such a measurement would be the axial-vector coupling constant associated with the semileptonic weak interaction of the neutral components of the isovector currents. This measurement would be to neutral currents what the measurement of the axial-vector coupling constant in the decay of ^{12}B, for example, is to charge-exchange currents. High-energy neutrino experiments are not nearly as reliable for the determination of a coupling constant, since induced tensor interactions, momentum-transfer-dependent form factors, and the presence of both vector and axial-vector interactions seriously complicate the interpretation. In the low-energy limit only the isovector axial-vector matrix element contributes, allowing the direct determination of that coupling constant alone.[6,8]

The prediction of the total cross section requires an accurate knowledge of the spectrum of antineutrinos from the β decays of the equilibrium fission products within the core of the source reactor. The total cross section can be defined as follows:

$$\bar{\sigma} \equiv \int_0^\infty \sigma(q) P(q) dq \,, \tag{2}$$

where $\sigma(q)$ is the reaction cross section for an incident antineutrino of energy q and $P(q)dq$ is the probability that any given antineutrino will have energy between q and $q+dq$. The quantity $P(q)$ is simply obtained from the antineutrino spectrum $N(q)$, discussed below, by straightforward normalization. The antineutrino spectrum given in this paper is a new version of our earlier spectra[9,10] and contains detailed decay-scheme information updated to early 1977. There is an increase of about 12% in the predicted value of $\bar{\sigma}$ when the present spectrum is used over that quoted in Ref. 6 which was calculated with the spectrum given in Ref. 9. This change is larger than the 10% accuracy which is predicted in the recently completed feasibility study described in Ref. 7. There are two recent conflicting values of $\bar{\sigma}$ in the literature, although both were calculated with the spectrum given in Ref. 9. Ahrens and Lang[6] give the value $\bar{\sigma} = 6.5 \times 10^{-45}$ cm^2, while Gurr *et al.*[11] give a value of $\bar{\sigma} = 4.4 \times 10^{-45}$ cm^2 based on the theoretical calculations of Gapanov and Tyutin.[5] The theoretical cross section of Gapanov and Tyutin, and of King and Ahrens were both weighted with the antineutrino spectrum again in the present work, and were found to give the same value of $\bar{\sigma} = 6.5 \times 10^{-45}$ cm^2 when weighted by the spectrum of Ref. 9, and the value of $\bar{\sigma} = 7.4 \times 10^{-45}$ cm^2 when weighted by the updated spectrum given in this paper. We have also

looked in detail at the results of the most recent theoretical treatment of this problem,[8] and it is easily shown that with a simple but important correction, both the differential and total cross sections of Ref. 8 are practically the same as those given in Refs. 5 and 6 when considered at low energy. An experimental upper limit on the cross section of $\bar{\sigma} = 2.64 \times 10^{-44}$ cm^2 is given in Ref. 11 which is a factor of 3.6 greater than the present theoretical value. This factor was quoted as 6 based on the theoretical total cross section ($\bar{\sigma} = 4.4 \times 10^{-45}$ cm^2) quoted in Ref. 11. We believe this latter value of $\bar{\sigma}$ to be in error.

II. THE THEORETICAL CROSS SECTION

In the two theoretical treatments of the antineutrino disintegration of the deuteron given by King and Ahrens, and by Gapanov and Tyutin,[5] the same general form of the Hamiltonian was used in which charge independence could be easily incorporated. In addition, the same allowed approximation was made which results in only the isovector, axial-vector interaction contributing through the matrix element of $\tau_3\vec{\sigma}$. In addition, the D-state contribution was neglected in the deuteron wave function in both of these treatments. The work by Gapanov and Tyutin[5] included a finite range correction, while such a correction was also included in the later work of Ahrens and Lang.[6] It is not surprising then that the differential cross sections $d\sigma(q)/dE_k$, in nucleon energy E_k, can easily be shown to be identical. The differential cross sections of both Gapanov and Tyutin[5] and Ahrens and Lang[6] were integrated numerically over E_k and found to be in excellent agreement with the integrated cross section $\sigma(q)$ given in closed form in Ref. 6. All of these cross sections give a total cross section of $\bar{\sigma} = 7.4 \times 10^{-45}$ cm^2 when folded into the present spectrum.

The calculations given in Ref. 8 are based on the theory of Weinberg and Salam, while in this case also the D-state contribution to the deuteron wave function was neglected. In the low-energy limit then the momentum-dependent form factors $F_1^{(3)V} = F_2^{(3)V} = 0$ and the expression for $d\sigma(q)/dE_k$ given in their equation (2.15) should reduce to those given in Refs. 5 and 6. We find, however, that it does not, and, in fact, numerical integration of their differential cross section over E_k differs from their plot of $\sigma(q)$, given in their Fig. 2, by a constant factor. This factor is found to be $(1 - \gamma r_{0t})^{-1}$, where $\gamma = (mE_d)^{1/2} = 45.71$ MeV and in which m is the reduced nucleon rest-mass energy and E_d is the binding energy of the deuteron ($E_d = 2.225$ MeV). The quantity r_{0t} is the triplet effective range ($r_{0t} = 0.008\,666\,13$ MeV^{-1}). Apparently this factor was introduced in making the approximation that the nuclear force has a zero effective range in the final state but has a finite effective range in the bound deuteron state. This inconsistency leads to an extra factor of $(1 - \gamma r_{0t})^{-1}$ in the differential cross section. Somehow this factor canceled in their analytical integration of $d\sigma(q)/dE_k$ over E_k, and the final result for $\sigma(q)$, plotted in their Fig. 2 of Ref. 8, is in agreement with the analytically integrated result of Ref. 6 and with the numerically integrated results of both Refs. 5 and 6. If the factor in question is removed and if the coupling constants are defined as in Ref. 6, the differential cross section of Ref. 8 can be written for low-energy antineutrinos, and for zero effective range, as follows:

$$\frac{d\sigma(q)}{dE_k} = \frac{2G^2}{\pi^2} \frac{m^{3/2}\gamma(\gamma a_s - 1)^2 E_k^{1/2}(q - E_d - E_k)^2}{(mE_k a_s^2 + 1)(\gamma^2 + mE_k)^2}, \quad (3)$$

which is in exact agreement with the corresponding results given in Refs. 5 and 6. In Eq. (3), a_s is the singlet scattering length (-0.1201 MeV^{-1}), and $G = 2.769 \times 10^{-22}$ cm^2/MeV. We have numerically integrated Eq. (3) over E_k, which requires no further approximation, and found that it reproduces Fig. 2 of Ref. 8 and gives the same total cross section as given by the expressions in both Refs. 5 and 6.

III. THE ANTINEUTRINO SPECTRUM

We have assumed, as in the earlier calculations,[9,10] that the antineutrino spectrum from a reactor core is that of the fission products of ^{235}U in secular equilibrium. The details of the general method of calculating the spectrum are given in Refs. 8 and 9 and will only be outlined here.

The number of antineutrinos of energy q per fission, per unit energy range, from the fission products in secular equilibrium is given by

$$N(q) = \sum_j Y_j(ZA) b_j P_j(q), \quad (4)$$

where $Y_j(ZA)$ is the total yield of the fission product of charge Z and mass A, which decays through the jth branch, b_j is the jth β branching ratio and $P_j(q)$ is the theoretical, allowed, Coulomb-corrected antineutrino spectrum normalized to give a total probability of unity. In the present work we have used an approximate relativistic Fermi function $F(q, Z, A)$ which is based on the original Bethe-Bacher approximation for the complex Γ function,[12] combined with the mass and finite-size correction factor used in Bhalla's more recent work.[13] A simplifying approximation is very important in this calculation because spectra of approximately 650 β decays are Coulomb corrected at each point for numerical integration

which means $F(q,Z,A)$ is used about 10^5 times. An accurate, iterative procedure for calculating the complex Γ function for this many computations is extremely time consuming and would require a reduction in the accuracy of numerical integration. With the above approximation, the Fermi function can be written as follows:

$$F(\eta,Z,A)=\frac{4(1+S/2)}{[\Gamma(3+2S)]^2}\left(\frac{2R(A)}{\hbar/m_0c}\right)^{2S}\frac{2\pi y}{1-e^{-2\pi y}} \times\{\tfrac{1}{4}[(1+\eta^2)(1+4\gamma^2)-1]\}^S , \quad (5)$$

where $S+1=[1-(Z\alpha)^2]^{1/2}$, $\gamma=\alpha Z$, $y=\gamma(1+\eta^2)^{1/2}/\eta$, $R(A)=1.2\times10^{-13}A^{1/3}$ cm, and η is the electron momentum in units of m_0c. The approximation for the complex Γ function used above was shown earlier to be far superior to the nonrelativistic approximation.[14] We find, for example, that for 2-MeV electrons at $Z=90$, the difference between an accurate calculation of the relativistic Fermi function and the nonrelativistic approximation is 92%, whereas, for the above approximation, the difference is 5%. The resulting changes in the antineutrino spectrum are small but observable and represent the elimination of a source of systematic error.

The sources for the fission yields and charge distributions, and β-decay Q values used for predicting the β shapes of decays associated with products of unknown decay schemes, are the same as those used in Ref. 10. A search of the literature shows that the changes in these parameters are not nearly as important as the effects produced by the new spectroscopy data. In addition we need rely far less on the theoretical prediction of β end-point energies and branching ratios because only 27% of the total yield of fission products is associated with nuclides of unknown decay schemes, whereas in the earlier treatments of Refs. 9 and 10 this figure was 65% and 49%, respectively. The new spectroscopy data consist of 26 new decay schemes containing 150 β branches and represent 22% of the total fission yield. The resulting fission spectrum of antineutrinos is shown in Fig. 1 and is also given in Table I for computational purposes along with the uncertainties propagated from uncertainties in the input data.

The quoted uncertainties are obtained by varying the values of the yields, β-decay Q values and charge distributions over their ranges of uncertainty and calculating the shift $\delta_i(q)$ in the spectrum of the ith β branch at energy q. The total uncertainty due to that parameter is then given by

$$\delta N(q)=\left\{\sum a_i[\delta_i(q)]^2\right\}^{1/2}, \quad (6)$$

where a_i is proportional to the product of the branching ratio and yield. These uncertainties for the errors in the various sets of parameters are then combined as independent errors.

IV. SUMMARY AND CONCLUSIONS

It can be argued that the measurement of the cross section for the disintegration of the deuteron, by low-energy electron antineutrinos, can independently yield the value of the isovector, axial-vector coupling constant of the weak neutral current. It was shown above that the differences in the total cross section $\bar{\sigma}$ given in Refs. 6 and 11, using the results of the earlier theoretical treatments of Refs. 5 and 6, are in fact the result of an error and that both predict the value given in Ref. 6 when the older antineutrino spectrum[9] is used. When the present spectrum is used, a value of $\bar{\sigma}=7.4\times10^{-45}$ cm^2 is predicted using the numerically integrated, differential cross sections

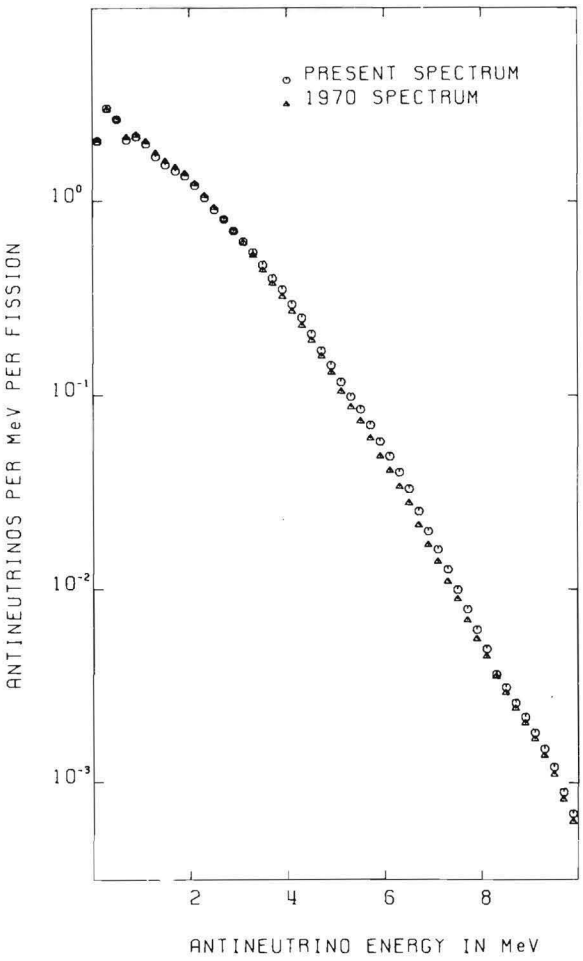

FIG. 1. Theoretical fission spectrum of antineutrinos.

TABLE I. Theoretical spectrum of antineutrinos from ^{235}U fission products in secular equilibrium. $N(q)$ is given in antineutrinos per MeV per fission.

q (MeV)	$N(q)$	q (MeV)	$N(q)$
0.2	3.87 ± 0.21	5.6	$(7.80 \pm 0.32) \times 10^{-2}$
0.4	2.80 ± 0.15	5.8	$(6.46 \pm 0.26) \times 10^{-2}$
0.6	1.98 ± 0.11	6.0	$(5.30 \pm 0.22) \times 10^{-2}$
0.8	2.12 ± 0.12	6.2	$(4.41 \pm 0.18) \times 10^{-2}$
1.0	2.06 ± 0.11	6.4	$(3.64 \pm 0.15) \times 10^{-2}$
1.2	1.90 ± 0.12	6.6	$(2.90 \pm 0.09) \times 10^{-2}$
1.4	1.59 ± 0.10	6.8	$(2.25 \pm 0.07) \times 10^{-2}$
1.6	1.47 ± 0.09	7.0	$(1.79 \pm 0.05) \times 10^{-2}$
1.8	1.39 ± 0.08	7.2	$(1.45 \pm 0.04) \times 10^{-2}$
2.0	1.27 ± 0.08	7.4	$(1.15 \pm 0.03) \times 10^{-2}$
2.2	1.13 ± 0.08	7.6	$(8.98 \pm 0.23) \times 10^{-3}$
2.4	$(9.78 \pm 0.60) \times 10^{-1}$	7.8	$(6.87 \pm 0.18) \times 10^{-3}$
2.6	$(8.60 \pm 0.52) \times 10^{-1}$	8.0	$(5.54 \pm 0.14) \times 10^{-3}$
2.8	$(7.65 \pm 0.52) \times 10^{-1}$	8.2	$(4.40 \pm 0.11) \times 10^{-3}$
3.0	$(6.57 \pm 0.47) \times 10^{-1}$	8.4	$(3.35 \pm 0.08) \times 10^{-3}$
3.2	$(5.86 \pm 0.42) \times 10^{-1}$	8.6	$(2.81 \pm 0.07) \times 10^{-3}$
3.4	$(5.11 \pm 0.36) \times 10^{-1}$	8.8	$(2.36 \pm 0.06) \times 10^{-3}$
3.6	$(4.41 \pm 0.31) \times 10^{-1}$	9.0	$(1.97 \pm 0.05) \times 10^{-3}$
3.8	$(3.76 \pm 0.27) \times 10^{-1}$	9.2	$(1.64 \pm 0.04) \times 10^{-3}$
4.0	$(3.23 \pm 0.23) \times 10^{-1}$	9.4	$(1.33 \pm 0.05) \times 10^{-3}$
4.2	$(2.72 \pm 0.19) \times 10^{-1}$	9.6	$(1.06 \pm 0.06) \times 10^{-3}$
4.4	$(2.28 \pm 0.16) \times 10^{-1}$	9.8	$(7.95 \pm 0.49) \times 10^{-4}$
4.6	$(1.91 \pm 0.14) \times 10^{-1}$	10.0	$(6.05 \pm 0.38) \times 10^{-4}$
4.8	$(1.57 \pm 0.11) \times 10^{-1}$	10.2	$(4.46 \pm 0.28) \times 10^{-4}$
5.0	$(1.30 \pm 0.09) \times 10^{-1}$	10.4	$(3.05 \pm 0.19) \times 10^{-4}$
5.2	$(1.09 \pm 0.08) \times 10^{-1}$	10.6	$(1.89 \pm 0.12) \times 10^{-4}$
5.4	$(9.17 \pm 0.65) \times 10^{-2}$		

$d\sigma(q)/dE_k$ of either Gapanov and Tyutin[5] or of Ahrens and Lang.[6] The low-energy limit of a recent treatment of the antineutrino disintegration of the deuteron in the framework of Weinberg and Salam theory, given by Ali and Dominguez,[8] was also investigated. It was found that their differential cross section $d\sigma(q)/dE_k$, when numerically integrated over E_k, did not reproduce their plot of $\sigma(q)$ until an erroneous factor of $(1-\gamma r_{0t})^{-1}$ was removed. Their differential cross section then is internally consistent and at low energy is equivalent to the zero-effective-range results given in the articles of Ref. 5.

Finally, an improved version of the spectrum of antineutrinos from the fission products of ^{235}U in secular equilibrium is presented. The improvement arises by including recently published, experimentally determined β-decay Q values and branching ratios of 150 β branches in 26 nuclei representing 22% of the total yield. In addition, a far more accurate approximation to the relativistic Fermi function was used in the calculation of each point of every individual antineutrino spectrum.

ACKNOWLEDGMENTS

One of the authors (F.T.A.) would like to thank T. P. Lang and also the School of Physics of the Georgia Institute of Technology for their hospitality during the later stages of this work. We would especially like to thank Professor Ahrens for his continued interest, his critical reading of the manuscript, and in particular for clarifying the discrepancies between the theoretical calculations.

*Work supported in part by NSF under Grant PHY 75-21295

[1]S. Weinberg, Rev. Mod. Phys. 46, 255 (1974).
[2]M. A. B. Beg and A. Sirlin, Annu. Rev. Nucl. Sci. 24, 379 (1974).
[3]E. S. Abers and B. W. Lee, Phys. Rep. 9C, 1 (1973).
[4]F. J. Hasert, *et al.*, Phys. Lett. 46B, 138 (1973); J. W. Chapman, *et al.*, Phys. Rev. D 14, 5 (1976).
[5]R. W. King and T. Ahrens, Advanced Research Corporation Report No. NRI-C, Lafayette, Indiana, 1962 (unpublished); Yu. V. Gapanov and I. V. Tyutin, Zh. Eksp. Teor. Fiz. 47, 1826 (1964) [Sov. Phys. JETP 20, 1231 (1965)]; T. Ahrens, C. P. Frahm, and Q. Bui Duy, Nucl. Phys. 78, 641 (1966).
[6]T. Ahrens and T. P. Lang, Phys. Rev. C 3, 979 (1971).
[7]T. P. Lang, S. M. Blankenship, J. R. House, T. Ahrens, D. S. Harmer, M. H. Wood, and F. T. Avignone III, report (unpublished).
[8]Ahmed Ali and C. A. Dominguez, Phys. Rev. D 12, 3673 (1975).
[9]F. T. Avignone III, S. M. Blankenship, and C. W. Darden, III, Phys. Rev. 170, 931 (1968).
[10]F. T. Avignone III, Phys. Rev. D 2, 2609 (1970).
[11]H. S. Gurr, F. Reines, and H. W. Sobel, Phys. Rev. Lett. 33, 1979 (1974).
[12]H. A. Bethe and R. F. Bacher, Rev. Mod. Phys. 8, 194 (1936).
[13]C. P. Bhalla, U. S. National Bureau of Standards, Monograph 81 (1964).
[14]I. Feister, Phys. Rev. 78, 375 (1950).

Appendix II

SCIENTIFIC COLLABORATORS

Co-Principal Investigators:

T. P. Lang, Principal Research Scientist

R. M. Ahrens, Professor of Physics

Collaborators:

F. T. Avignone, Professor of Physics (Univ. of South Carolina)

S. M. Blankenship, Research Scientist

D. S. Harmer, Professor of Physics and Nuclear Engineering

J. R. House, Assistant Research Scientist

A. M. Rushton, Adjunct Professor of Physics

R. M. Wood, Graduate Student of Physics